A fractional differential scheme for the effective transport properties of multiscale reactive porous media: Applications to clayey geomaterials

Philippe Cosenza, Richard Giot, Albert Giraud, Stephen Hedan

A Fractional Differential Scheme for the Effective Transport Properties of Multiscale Reactive Porous Media: Applications to Clayey Geomaterials

Philippe COSENZA[(1)*], Richard GIOT[(1)], Albert GIRAUD[(2)], Stephen HEDAN[(1)]

(1) University of Poitiers (ENSI Poitiers), CNRS, UMR 7285 IC2MP- HydrASA, Poitiers, France.

(2) University of Lorraine (ENSG), CNRS, CREGU, GeoRessources Laboratory, Vandoeuvre-les-Nancy, France

*** Corresponding author**

Philippe COSENZA

Ecole Nationale Supérieure d'Ingénieurs de Poitiers (exESIP)
Université de Poitiers-CNRS
1 rue Marcel Doré, Bat B1
TSA 41105
86073 Poitiers cedex 09
France
Email: philippe.cosenza@univ-poitiers.fr

Intended for publication in International Journal for Numerical and Analytical Methods in Geomechanics

Abstract

A new homogenization scheme is proposed to model the effects of surface phenomena occurring at the pore fluid/solid interface on the effective transport properties of multiscale and reactive geosystems, e.g., clayey geomaterials. This new scheme is a generalization of the so-called differential scheme (DS) used to infer the effective properties of a composite made up of several materials. It is named the fractional differential scheme and is based on two key elements: (i) the concept of realizability of the DS itself and (ii) a fractional integral formulation of the DS for a porous medium considered as a two-component composite. The formulation of the fractional DS introduces two parameters: a cementation exponent m and a fractional order α. The cementation exponent m is related to the microstructure of the material. The fractional order α accounts for the amplitude of the "surface" transport of ions resulting from the physico-chemical interactions between hydrated cations and swelling clay minerals. Both parameters m and α are inverted from two sets of data: electrical conductivity measurements obtained on clayey rocks and effective diffusion coefficient measurements acquired from a Na-montmorillonite geomaterial. The inversion results demonstrate that the fractional DS model is able to capture the dependence of the cation concentration on the effective transport properties of the clayey materials under study. Our results also show that the fractional order α can be considered an indirect indicator of the amplitude of physico-chemical interactions between hydrated cations and swelling clay minerals occurring at the pore fluid/solid interface.

Keywords: differential scheme, fractional integral, clayey geomaterials, transport properties, electrical conductivity, diffusion coefficient, reactive porous media.

1. Introduction

There are different approaches for estimating the effective properties of a composite made up of several materials. Rigorous procedures exist for composites with well-characterized or ideal (i.e., periodic) microstructures (e.g., [1]). However, these procedures are not applicable when the underlying microstructure is random or multiscale. In this case, the typical approach is to use one of several "effective medium approximations" (EMAs). Among these approximations are the self-consistent approximation (SCA) and the differential scheme (DS), which differ in the way in which they treat the components constituting a symmetric or nonsymmetric basis in the final equations[2]. SCA was developed for polycrystalline microstructures or N-component composites where all components are treated equally, with no one material identified as the host to be described. In contrast to SCA, the DS does not treat the components equally. In the simplest case of a two-component composite, one component is taken as the host and the other, considered to be an inclusion, is added incrementally "in a such a way that the newly added material is always in dilute approximation with respect to the current effective medium"[3]. Reviews of the relevant studies on these EMAs can be found in Hashin[4], Berryman[5] and Böhm[1]. We note that SCA is also known as the symmetrical effective medium theory, the coherent potential approximation, or simply the effective medium approximation; the DS is known as the unsymmetrical effective medium theory, iterated dilute approximation, self-similar model, or differential effective medium scheme[6-11].

The DS is particularly popular in geophysics because it predicts the empirical Archie relationships for the effective electrical conductivity of rocks[6, 12] and for the effective diffusion coefficient of geomaterials[13-15]. Moreover, the DS approach is widely and successfully used to model the following properties of sedimentary rocks and soils: (1) elastic properties related to seismic velocities[10, 16-19] and (2) dielectric properties for a wide range of frequencies[20-26]. It should be noted that a major part of the geomaterials involved in these studies are often seen as

saturated random porous media or simply as two-phase composites composed of a pore solution and solid grains. More recently, the DS approach has been modified to quantify the effective properties of a composite material near the percolation thresholds of different physical types[15, 27-29].

Despite its ability to model the effective transport properties of porous geomaterials, the DS has not been conceptually designed to account for complex physico-chemical interactions existing in the pore solution in contact with the solid phase, such as cation exchanges, electrostatic attractions/repulsions or surface complexation reactions, among others. A few attempts have been made to overcome this conceptual difficulty and to integrate all these surface effects into DS approaches. In these approaches, all the surface phenomena are brought together to be encapsulated in a "grain" property, sometimes through a theoretical physico-chemical approach, e.g., electrical double or triple layer theory[12, 25, 30-31]. This "grain" property, which is not a proper interface property, accounts for both the surface conduction and other interactions occurring at the fluid/grain interface and the transport inside the solid grain, which is mostly negligible in practice. We note that all these DS contributions deal with clayey geomaterials that are especially rich in smectite clay minerals containing a substantial excess of fixed negative charges, which must be compensated by dissolved counter cations. The presence of these charged clay minerals and their associated dissolved counter cations originate from the so-called electrical double (or triple) layer existing in these minerals at nanopore scale (typically a few nanometers)[32].

Moreover, it should be mentioned that EMAs different from the DS exist, where all the physico-chemical phenomena at the surface can be embedded in an additional interfacial zone, spatially separated from the solid-grain phase and the fluid-pore phase[33-34]. However, as far as we know, these EMAs have not been validated on data acquired from dense porous materials or even from geomaterials.

In this paper, a new DS is developed and used to quantify the effects of surface physico-chemical phenomena occurring at the pore fluid/solid interface on the effective transport properties of reactive geosystems, e.g., clayey materials. This new scheme, which requires neither a particular "grain" transport property nor an interfacial zone, is based on two key elements: (i) the realizability of the DS itself and (ii) an integral formulation of the DS for two-component composites. Regarding the first element, an EMA is called realizable if we can describe a construction process that makes a composite with effective property predicted by the corresponding theory[3, 5, 35]. In the case of the DS, for a two-component composite of materials 1 and 2, the construction process starts with a matrix of component 1, for instance, and embedded inclusions of phase 2 in dilute concentration. The next stage involves embedding the grains of component 2 that are, in terms of size, an order of magnitude larger than the previous ones, and this process continues until component 2 occupies its assigned volume fraction (e.g., [3,36]). This construction process leads to a multiscale or "fractal-like" microstructure constituted by a set of many inclusions of many orders of magnitude. Note that this textural or microstructural feature is typical of clayey materials[37-41].

Regarding the second key element, the integral formulation of the DS for a two-component composite allows us to introduce the kernel of the Riemann-Liouville integral with a fractional exponent that is related to the amplitude of additional interactions occurring between the solid inclusions themselves and the pore solution. The amplitude of these additional interactions can be modulated in the construction process previously described, following the sizes of the added inclusions. As explained further, these additional interactions, which can be amplified even for the smallest solid inclusions, i.e., at nanoscale, are interpreted as physico-chemical interactions occurring in the considered reactive porous medium.

The theoretical foundations of this new DS, hereafter called the fractional DS, are presented in the first section of this paper. In the second part, this fractional DS is used and

tested on transport properties data taken from the literature, i.e., electrical conductivity and diffusion coefficient acquired from clayey geomaterials.

2. Theoretical background

2.1 differential scheme: a realizable scheme for multiscale materials

In this section, the theoretical basis of the DS is briefly recalled. Let us consider the simplest case: a two-component composite made of grains or inclusions named phase 2 embedded in a matrix called phase 1. It is well known, e.g., from Hashin[42], that when this two-component material is subjected to the average gradient $\bar{G}$ of a state variable (e.g., the voltage gradient/electrical field, concentration gradient, or temperature gradient), the effective conductivity tensor $\boldsymbol{K}^*$ is expressed as follows:

$$\boldsymbol{K}^* = \boldsymbol{K}_1 + (\boldsymbol{K}_2 - \boldsymbol{K}_1)\boldsymbol{A}\,\phi_2 \tag{1}$$

where $\boldsymbol{K}_1$ and $\boldsymbol{K}_2$ are the conductivity tensors of the components that have the volume fractions ϕ_1 and ϕ_2, respectively, and the so-called concentration tensor $\boldsymbol{A}$ is defined by:

$$\bar{G}_2 = \frac{1}{V_2}\int_{V_2} G\,dV = \boldsymbol{A}\bar{G} \tag{2}$$

G is the actual gradient throughout V_2, which is the volume occupied by the included phase within a representative volume range[42-43]. In the case of small concentrations, i.e., $\phi_2 \ll 1$, in which it is assumed that the inclusions are fully isolated with no interaction with each other, it can be shown that the concentration tensor $\boldsymbol{A}$ is only a function of the conductivity tensors of the components and the geometrical parameters of the inclusions g:

$$\boldsymbol{A} = \boldsymbol{A}(\boldsymbol{K}_1, \boldsymbol{K}_2, g) \tag{3}$$

Note that for inclusions with simple geometries (i.e., spheres, spheroids, and ellipsoids), the tensor $\boldsymbol{A}$ can be written in an analytical way[1, 4, 5].

Following the DS, which is an iterative process, the effective property of the composite is explicitly calculated from an initial material through a series of incremental additions of

inclusions or elementary units. In our case where we have a two-component composite, the procedure begins with the initial material 1 corresponding to a conductivity $\boldsymbol{K_1}$ in a volume V_0. A small fraction of inclusions 2, $\delta\phi_2$, is embedded in matrix 1, and the effective conductivity of this mixture is calculated relative to a dilute suspension of particles 2 in matrix 1 (i.e., equations (1) and (3)). Now, in the volume V_0, the mixture has a homogenized effective conductivity $\boldsymbol{K^*}$ and constitutes the initial matrix of the next step, during which a new small fraction of inclusions 2, $\delta\phi_2$, is embedded. The homogenized effective conductivity $\boldsymbol{K^*}$ of this new mixture with a fraction of inclusions 2 ($\delta\phi_2$) is calculated, and the construction process continues until: (1) at each stage, the embedded inclusion 2 is in dilute concentration and (2) the required volume ratio of the inclusions is satisfied.

This construction process can be mathematically described by a differential equation. Indeed, since at each step of this construction process, a small concentration of inclusions is added ($\delta\phi_2 << 1$) the dilute approximation (equations (1) and (3)) holds:

$$\boldsymbol{K}^*(\phi_2 + \delta\phi_2) = \boldsymbol{K}^*(\phi_2) + \left(\boldsymbol{K}_2 - \boldsymbol{K}^*(\phi_2)\right)\boldsymbol{A}\,(\boldsymbol{K}^*(\phi_2), \boldsymbol{K}_2, g)\delta\phi_2 \tag{4}$$

Thus, for the limit $\delta\phi_2 \to 0$, equation (4) yields the following differential equation:

$$\frac{d\boldsymbol{K}^*}{d\phi_2} = (\boldsymbol{K}_2 - \boldsymbol{K}^*)\boldsymbol{A} \tag{5}$$

which must be solved with the initial condition:

$$\boldsymbol{K}^*(\phi_2 = 0) = \boldsymbol{K_1} \tag{6}$$

As shown by McLaughlin[44], $\delta\phi_2$ is not the proper equivalent of a small concentration of inclusions in equation (4), but $\delta\phi_2/(1-\phi_2)$ is instead. Since the inclusions are assumed to be dispersed randomly in the matrix, the added inclusions for a given step essentially replace matrix material, but they also replace a portion of the previously added inclusions: only a fraction ϕ_1 (or $1-\phi_2$) of $\delta\phi_2$ contributes to the increase in ϕ_2 in the DS construction process. This remark results in the following differential initial value problem [44]:

$$\frac{d\boldsymbol{K}^*}{d\phi_2} = \frac{(\boldsymbol{K_2} - \boldsymbol{K}^*)}{1-\phi_2}\boldsymbol{A}\,, \qquad \boldsymbol{K}^*(\phi_2 = 0) = \boldsymbol{K_1} \tag{7}$$

To our knowledge, the physical interpretation of the DS construction process and the associated differential initial value problem has been provided by Roscoe[36]. Following Roscoe's interpretation, the microgeometries or microstructures of the composites associated with the DS are made up of many inclusions of many orders of magnitude. The main physical idea can be seen in equation (4), which states that the added inclusions at a given step of the construction process "see" an effective medium. If the added inclusions "see" an effective medium, then it means that these inclusions are much larger than the current ones. In fact, following this physical interpretation, the construction process can be considered as a filling process that begins with the smallest inclusions and continues in increasing order of magnitude to obtain *in fine* a multiscale or "fractal-like" microstructure. According to many authors[3, 5, 7, 8], the existence of such microgeometry characterizes the DS as a realizable scheme.

As illustration, the previous differential initial value problem (7) can be rewritten for randomly oriented spheroidal inclusions (e.g., ellipsoids of revolution) embedded in an isotropic matrix[11, 45]:

$$\frac{dk^*}{d\phi_2} = \frac{(k_2 - k^*)}{1-\phi_2}\frac{k^*}{3}\sum_{i=x,y,z}\frac{1}{k_2 L_i + k^*(1-L_i)}, \qquad k^*(\phi_2 = 0) = k_1 \tag{8}$$

where k^*, k_1 and k_2 are the overall scalar effective conductivity, the scalar conductivity of component 1 and the scalar conductivity of component 2, respectively. The depolarization factors L_i of the spheroidal inclusions obey the following equations:

$$L_z = L\,,\; L_x = L_y = \frac{1}{2}(1-L) \tag{9}$$

The value of L is determined by the eccentricity e of the spheroid. For prolate spheroids with semiaxes ($a_x > a_y = a_z$), L is given by[46]:

$$L = \frac{1-e^2}{2e^3}\left(ln\frac{1+e}{1-e} - 2e\right) \tag{10}$$

189 with

$$e = \sqrt{1 - \frac{a_y^2}{a_z^2}} \tag{11}$$

190 while for oblate spheroids with $a_x=a_y>a_z$, L becomes:

$$L = \frac{1 + e^2}{e^3}(e - tan^{-1}e) \tag{12}$$

191 with

$$e = \sqrt{\frac{a_y^2}{a_z^2} - 1} \tag{13}$$

192 For spherical inclusions, the depolarization factors are simply given by:

$$L_z = L_x = L_y = \frac{1}{3} \tag{14}$$

193 Note that the differential initial value problem (7) can also be written for the general
194 anisotropic case, for which the phases are anisotropic materials[47].

195 In the following, the porous media of interest are composed of insulating grains, i.e.,
196 $k_2=0$, and the electrolyte-filled pores are viewed as matrix 1. In this case, the previous
197 differential initial value problem (8) can be simplified as follows:

$$\frac{dk^*}{d\phi} = m\frac{k^*}{\phi}, \qquad k^*(\phi = 1) = k_1 = k_w \tag{15}$$

198 where for the sake of lightening notation, $\phi=\phi_1=1-\phi_2$ is the porosity, k_w is the water conductivity
199 or the electrolyte conductivity of the pores, and the parameter m, often called the "cementation
200 exponent", is given by [45, 48-49]:

$$m = \frac{5 - 3L}{3(1 - L^2)} \tag{16}$$

201 For spherical grains, it is easy to check that $m=1.5$ by using equations (14) and (16).

202 The differential initial value problem can also be expressed in the following integral form:

$$\int_{k_w}^{k^*} \frac{dk}{k} = m \int_{1}^{\phi} \frac{dv}{v} = -m \int_{0}^{\phi_2} \frac{d\phi}{1-\phi} \tag{17}$$

The integration of (17) leads to the so-called Archie relationship:

$$k^* = k_w \phi^m = \frac{k_w}{F} \tag{18}$$

where *F*, called the formation factor, is defined by

$$F = \frac{k_w}{k^*} = \phi^{-m} \tag{19}$$

or

$$lnF = -m\ ln\phi \tag{20}$$

The term "formation factor" was originally used by Archie because it was approximately constant for any given geological formation. Regarding its physical meaning, the formation factor, and particularly the cementation exponent *m*, are inextricably related to the concept of tortuosity, a term used to define the connectivity of the pore space as it affects transport processes through porous media[50-51]. The cementation exponent *m* intrinsically associated with the concept of the formation factor is clearly a microstructure-dependent parameter of porous media[52-53].

Although Archie's relationship (18) was derived from electrical measurements on a relatively small number of only a few types of sedimentary rocks, it has been successfully used for a wide range of porous media and for diffusion coefficients[13-14]. All these porous media are made up of a nonconductive mineral skeleton immersed in a single conductive phase, i.e., a liquid that completely saturates the connected pore space[54]. However, Archie's relationship is no longer valid for geomaterials such as clay materials containing nanopores of only a few nanometers in length that are filled with an electrolyte possessing special transport properties. These particular transport properties, existing at nanopore scale, result from complex surface physico-chemical phenomena occurring at the liquid-mineral interface; these include chemical reactions at mineral surface sites, electrostatic interactions between the surface and ions,

wettings, and electrokinetic couplings[55-57]. All these surface physico-chemical phenomena often refer to surface conduction[12, 30, 32, 58] or surface diffusion[59-60]. To account for this surface transport, the previous DS that led to Archie's relationship is modified by introducing concepts from fractional calculus, as explained in the next section.

2.2 A fractional differential scheme

We focus on the last case presented in the previous section, i.e., a porous medium viewed as a two-component composite made of nonconductive grains immersed in a single conductive liquid. Following the DS approach, the effective transport property of a such composite is governed by equations (15) or (17), which can be expressed in an incremental way as follows:

$$k^*_{(i+1)} = k^*_{(i)}\left(1 - m\frac{\delta\phi_2}{1-\phi_{2\,(i)}}\right) \tag{21}$$

where $k^*_{(i+1)}$ and $k^*_{(i)}$ are the effective properties at steps *(i+1)* and *(i)* in the DS construction process, respectively. The quantity $\frac{\delta\phi_2}{1-\phi_{2\,(i)}}$ is the volumetric amount of grains added in the effective medium of property $k^*_{(i)}$ to obtain the property at step *(i+1)*.

Equation (21) is interesting because it combines two concepts: the differential initial value problem (15) and the construction process underlying the DS approach. In equation (21), the term in brackets on the right-hand side can be considered an "interaction term". At a given step of the construction process, it defines the interactions between the added inclusions and the current ones. Following the DS construction process, the sum of all these interactions ultimately leads to Archie's relationship (18) associated with a given transport mechanism, i.e., a "bulk" transport in the connected conductive/diffuse phase immersing a nonconductive/non-diffuse multiscale solid skeleton.

Consequently, if we want to introduce a new transport mechanism, i.e., one associated with surface conduction or surface physico-chemical phenomena, then the interaction term in

(21) has to be modified. The simplest way to modify this term is to introduce a weighted coefficient $K_{(i)}$ that evolves during the DS construction process:

$$k^*_{(i+1)} = k^*_{(i)}\left(1 - mK_{(i)}\frac{\delta\phi_2}{1-\phi_{2\,(i)}}\right) \tag{22}$$

Following Roscoe's interpretation of the DS, if we want to introduce new interactions between inclusions at the smallest scale, one may expect high values of $K_{(i)}$, i.e., much larger than 1, at the beginning of the filling process, i.e., at small values of (i), for the smallest inclusions. It should be noted that this coefficient could have been introduced upstream in the initial Eshelby problem.

The incremental equation (22) can also be reformulated in the following integral form:

$$\int_{k_w}^{k^*}\frac{dk}{k} = -m\int_0^{\phi_2} K(u)\frac{du}{1-u} \tag{23}$$

where the kernel $K(u)$ must be defined.

In this work, the following candidate is chosen:

$$K(u) = \frac{\alpha(\phi_2-u)^{\alpha-1}}{\phi_2^{\alpha-1}} \tag{24}$$

This choice is interesting for at least two reasons. First, the numerator $(\phi_2-u)^{\alpha-1}$ allows the introduction of the fractional calculus formalism, i.e., the Riemann-Liouville (RL) fractional integral:

$$\int_0^{\phi_2}\frac{\alpha(\phi_2-u)^{\alpha-1}}{\phi_2^{\alpha-1}}\frac{du}{1-u} = \frac{\alpha}{\phi_2^{\alpha-1}}\frac{\Gamma(\alpha)}{\Gamma(\alpha)}\int_0^{\phi_2}\frac{(\phi_2-u)^{\alpha-1}\,du}{1-u} = \frac{\alpha\Gamma(\alpha)}{\phi_2^{\alpha-1}}\;{}_0D_{\phi_2}^{-\alpha}f(\phi_2) \tag{25}$$

where Γ is the gamma function and $f(\phi_2) = \frac{1}{1-\phi_2}$. The quantity ${}_0D_{\phi_2}^{-\alpha}f(\phi_2)$ or ${}_0D_{\phi_2}^{-\alpha}\left(\frac{1}{1-\phi_2}\right)$ is the RL fractional integral of the function $1/(1-\phi_2)$ of order α. Recall that the RL fractional integral of the function $f(\phi_2)$ is defined by[61]:

$$ {}_0D_{\phi_2}^{-\alpha} f(\phi_2) = \frac{1}{\Gamma(\alpha)} \int_0^{\phi_2} f(u)\,(\phi_2 - u)^{\alpha-1} du \tag{26} $$

261 Or, in our case:

$$ {}_0D_{\phi_2}^{-\alpha} \left(\frac{1}{1-\phi_2}\right) = \frac{1}{\Gamma(\alpha)} \int_0^{\phi_2} \frac{1}{1-u}\,(\phi_2 - u)^{\alpha-1}\, du \tag{27} $$

262 The parameter α, the order of the RL integral, obeys the inequality $\alpha \geq 1$, but this
263 condition can be generalized to $\mathrm{Re}(\alpha)>0$ if the integral in (27) is an improper Riemann integral
264 (Miller and Ross, 1993).

265 The main advantage of this particular choice lies in the parameter α, which introduces
266 a certain flexibility to the kernel $K(u)$. Note that if $\alpha>1$, the kernel $K(u)$ is a monotonically
267 decreasing function of ϕ, meaning that $K(u)$ is at its maximum at the beginning of the integral
268 path in (23) and thus at the beginning of the DS filling process, when the added inclusions are
269 the smallest. At this stage, parameter α can be seen as "potentiometer" which controls through
270 the kernel $K(u)$ the amplitude of physico-chemical interactions between the added inclusions
271 in the DS filling process. As discussed further through an inverse modeling approach, the
272 fractional order α can be interpreted as an indirect indicator of the amplitude of physico-
273 chemical interactions occurring at the pore fluid/solid interface in clayey geomaterials.

274 Second, the denominator $\phi_2^{\alpha-1}$ satisfies the following normalization condition:

$$ \frac{1}{\phi_2} \int_0^{\phi_2} K(u) du = 1 \tag{28} $$

275 that is easy to check.

276 From (24) and (25), the integral formulation of the DS (23) can be rewritten as follows:

$$ ln\left(\frac{k_w}{k^*}\right) = m \frac{\alpha\Gamma(\alpha)}{\phi_2^{\alpha-1}}\ {}_0D_{\phi_2}^{-\alpha} \left(\frac{1}{1-\phi_2}\right) \tag{29} $$

277 Or, by introducing the formation factor $F = k_w/k^*$ and the porosity $\phi = 1 - \phi_2$:

$$\ln F = m\frac{\alpha\Gamma(\alpha)}{(1-\phi)^{\alpha-1}}\ {}_0D_{1-\phi}^{-\alpha}\left(\frac{1}{\phi}\right) \tag{30}$$

278 In contrast with Archie's relationship (20), the formation factor *F* now depends (i) on
279 the porosity ϕ through the RL fractional integral and (ii) on the fractional order α. Equation
280 (29) defines a fractional DS of a two-phase composite, i.e., a porous medium made of a
281 connected conductive phase immersing a nonconductive multiscale solid skeleton.

282 Equation (30) can be rewritten in a simpler way by introducing the incomplete beta
283 function $B_x(a,b)$:

$$B_x(a,b) = \int_0^x u^{a-1}\,(1-u)^{b-1}du \quad (a,b>0) \tag{31}$$

284 and by using the following relationship[61]:

$${}_cD_t^{-\nu}(a-t)^{\lambda} = \frac{(a-t)^{\lambda+\nu}}{\Gamma(\nu)}B_\tau(\nu;-\lambda-\nu)\,, \qquad \tau = \frac{t-c}{a-c} \tag{32}$$

285 If we set *c=0*, *t=1-*ϕ, *a=1*, λ*=-1*, ν=α, equation (32) becomes:

$${}_0D_{1-\phi}^{-\alpha}\left(\frac{1}{\phi}\right) = \frac{\phi^{\alpha-1}}{\Gamma(\alpha)}B_{1-\phi}(\alpha;1-\alpha) \qquad \tau = 1-\phi \tag{33}$$

286 and thus equation (30) yields

$$\ln F = m\,\alpha\left(\frac{\phi}{1-\phi}\right)^{\alpha-1} B_{1-\phi}(\alpha;1-\alpha) \tag{34}$$

287 or

$$\ln F = m\,\Psi(\phi,\alpha) \tag{35}$$

288 with

$$\Psi(\phi,\alpha) = \alpha\left(\frac{\phi}{1-\phi}\right)^{\alpha-1} B_{1-\phi}(\alpha;1-\alpha) \tag{36}$$

289 From the definition of the formation factor $F = k_w/k^*$, the effective transport property k^* is
290 thus given by:

$$k^* = k_w\, e^{-m\Psi(\phi,\alpha)} \tag{37}$$

At this stage, three comments can be made. First, equations (34) and (37) are easier to handle than equation (30) because the beta incomplete function has been widely studied in the mathematical literature, especially in statistics. Indeed, the beta incomplete function is available for all Excel-type spreadsheets and thus can be calculated easily without having to write any programs. This means that despite the apparent complexity of equations (34) and (37), the effective conductivity k^* can be explicitly and directly calculated in a simple way.

Second, it is easy to check that for $\alpha=1$, equation (34) becomes:

$$\ln F = -m\, ln\phi \tag{38}$$

(note that $B_{1-\phi}(1;0) = -ln\phi$). Thus, Archie's relationship (20) is obviously retrieved.

Third, the interesting asymptotic case $\alpha >> 1$ can also be studied by using the following Newtonian result[61-62]:

$$B_x(a,b) = \int_0^x u^{a-1}\,(1-u)^{b-1}du = \frac{x^a(1-x)^b}{a}\mathcal{F}(a+b,1;a+1;x)) \tag{39}$$

where $\mathcal{F}$ is the hypergeometric series given by[63]:

$$\mathcal{F}(\alpha_1,\alpha_2;\alpha_3;x) = 1 + \frac{\alpha_1\alpha_2}{\alpha_3}\frac{x}{1!} + \frac{\alpha_1(\alpha_1+1)\alpha_2(\alpha_2+1)}{\alpha_3(\alpha_3+1)}\frac{x^2}{2!} \tag{40}$$

$$+ \frac{\alpha_1(\alpha_1+1)(\alpha_1+2)\alpha_2(\alpha_2+1)(\alpha_2+2)}{\alpha_3(\alpha_3+1)(\alpha_3+2)}\frac{x^3}{3!} + \cdots$$

For $x=1-\phi$, $a=\alpha$, $b=1-\alpha$ and for a large α, equations (40) and (39) give $\mathcal{F}(1,1;\alpha+1;1-\phi)\sim 1$ and $B_{1-\phi}(\alpha,1-\alpha)\sim\frac{\phi^{1-\alpha}(1-\phi)^{\alpha}}{\alpha}$. Thus, the formation factor in (34) is simply:

$$\ln F \sim m\,(1-\phi) \tag{41}$$

or

$$F \sim e^{m\,(1-\phi)} \tag{42}$$

Equation (42) provides two results. First, similar to Archie's relationship, for a high-porosity medium ($\phi\sim 1$), the formation factor F tends toward unity and therefore, $k^*\sim k_w$.

Second, for a low-porosity medium ($\phi \sim 0$), F tends toward a finite value e^m and therefore, $k^* \sim k_w e^{-m}$. This unexpected result shows that even if the porous medium is mainly constituted of a nonconductive solid, it is still significantly conductive with a conductivity function of k_w, that is, equal to $k_w e^{-m}$. This physical inconsistency with regard to the initial assumptions highlights that our DS approach should not be used for very low-porosity media associated with large values of α.

2.3 Analysis of the sensitivity lnF to the fractional order α

The fractional DS introduces a new parameter, i.e., the fractional order α, whose influence on the effective formation factor *F*, especially on the effective property *k**, must be investigated.

This sensitivity analysis is conducted by calculating *lnF* as a function of the parameter α over a wide range of porosity and cementation exponent values (equation (34), (35), or (36)). The porosity range used here is from 0.05 to 0.4 (i.e., 5-40%) and is representative of a large class of clayey porous media. The cementation exponent *m* ranges between 0.2 and 2.7. These lower and upper limits are taken from Revil et al.[32] and Dashtian et al.[64].

Figure 1 displays the results of this sensitivity analysis for the ranges of both the porosity ϕ and the cementation exponent *m*. This plot indicates the following results:

- *lnF* significantly changes as the value α values changes incrementally from 1 to 10, regardless of the values of ϕ and *m*. For α values greater than 100, *lnF* is almost constant and tends toward the asymptotic limit $m\ (1-\phi)$, as established previously (see equation 41).
- The sensitivity of *lnF* to α is largest for the smallest porosity values, all things being equal.
- The sensitivity of *lnF* to α is strongly influenced by the cementation exponent *m*. There exists almost a full order of magnitude between the *lnF* values of the

left vertical scale and those of the right vertical scale. This strong sensitivity is obviously due to the fact that lnF is directly proportional to m, all things being equal (see equation (34), (35), or (36)); there is indeed an order of magnitude between both m limits, i.e., between 0.2 and 2.7.

These results are confirmed by a $logF$-$log\phi$ plot, which is usually used in petrophysics to illustrate departures from Archie's relationship (Figure 2). These departures are interpreted as being due to the existence of electrical surface conduction associated with clay minerals, as evidenced from electrical resistivity measurements acquired for a large class of clayey geomaterials[31, 58, 65-66.] Figure 2 also displays the numerical results obtained from an empirical model[55] based on the well-known experimental results obtained from clayey rocks by Waxman [58,67].

In comparison with Figure 1, Figure 2 provides two additional results. First, it shows that the fractional DS is able to describe, at least qualitatively, the "curvilinear" trend observed in a $logF$-$log\phi$ relationship associated with surface conduction. The shape and amplitude of this "curvilinear" trend are clearly controlled by the value of the fractional order α. Small deviations from the unity value of α, i.e., α=1.2, induce significant deviations from Archie's relationship.

Second, the empirical model indicates that surface conduction in clay rocks significantly depends on the amplitude of liquid conductivity. The F-ϕ relationship must reflect this dependence, as the fractional DS cannot do so directly (see equation 34). Thus, this comparison with experimental data strongly suggests that the fractional order α should itself depend on the liquid conductivity k_w. In other words, in the theoretical framework of the fractional DS, an additional relationship linking α and k_w should be introduced. This observation is not surprising because most surface physico-chemical phenomena occurring at the solution/solid interface, e.g., the electrical double (triple) layer, are controlled by the concentrations of ions in solution (such as salinity), which in turn depend on the solution conductivity (at least the electrical

solution conductivity)[32]. Now, if the fractional order α is supposed to reflect the amplitude of the interfacial solid-pore interactions, then it must also depend in some way on the concentrations of ions and therefore on the solution conductivity. This dependence is illustrated in the following applications.

3. Applications

3.1 Clayey geomaterials as multiscale and reactive materials

Data on transport properties, mainly the electrical conductivity and diffusion coefficients of clayey materials, are now compared to predictions obtained from the fractional DS presented in the previous section (i.e., equations (34), (35) and (36)). Here, it is worth remembering that clayey materials are involved in many geoenvironmental issues. These geological materials are studied as natural or engineered barriers for deep geological radioactive waste repositories and form the main geological caps of many hydrocarbon reservoirs.

Clayey materials are preferred here for at least two reasons. First, as previously mentioned, clayey soils or rocks often show microstructural patterns that are observed in multiscale materials[37-41, 68]. They exhibit a complex hierarchical organization at microstructural levels observed with space scales of several orders of magnitude, typically from nanometers to millimeters[69]. Despite the technical difficulty of acquiring these observations, recent quantitative petrography studies showed that the histograms of nonclay grain sizes[71-72] (Figure 3a) and pore sizes[39, 72] (Figure 3b) obey, at the first order, a power law for a wide range of sizes of heterogeneities, ranging from micrometric size to one tenth of a millimeter. Thus, these results attest to the existence of a multiscale or “fractal-like” system or microstructure composed of a set of many heterogeneities of many sizes, and this system is the main textural signature associated with the DS.

Second, clay-rich materials are known to be reactive porous media, i.e., porous media where complex physicochemical interactions between the pore solution and solid-phase occur.

382 This reactivity is mainly due to the existence of smectite clay minerals containing a substantial
383 excess of fixed negative charges that have to be neutralized by dissolved counter cations. The
384 presence of these charged clay minerals and their associated dissolved counter cations originate
385 from the so-called electrical double (or triple) layer existing on these minerals at nanopore scale
386 (typically a few nanometers)[32]. Moreover, the presence of nanopores between the clay minerals
387 induces the existence of “bound” water or “interlayer” water with thermodynamic,
388 hydrodynamic and spectroscopic properties that appear close to those of ice[73]. In this interlayer
389 space, these water molecules can organize themselves in the form of (up to three) molecular
390 layers[74]. These adsorbed water molecules are subjected to physicochemical forces of a complex
391 nature: electrostatic attraction or repulsion, hydration or "structural" forces of the Derjaguin
392 type[75]. The upscaling of these physicochemical interactions and their associated transport
393 processes up to the (sample) scale of the engineer is obviously a challenging issue[57].

394 *3.2 Electrical conductivity of clay rocks*

395 The fractional DS is now applied to electrical conductivity data of water-saturated clayey rocks
396 taken from the database compiled by Waxman and Smits[58].

397 In the first stage, five samples from this database are selected to obtain a wide
398 distribution of cation exchangeable capacity (CEC) values. CEC is usually expressed in
399 milliequivalents per 100 g of dry material and quantifies the exchangeable cations neutralizing
400 negative charges in porous material[76]. A high CEC value for a given porous medium is
401 interpreted as the medium having a high potential for adsorption of hydrated cations at the
402 solution-mineral interface. Consequently, CEC can be considered for use with swelling clayey
403 materials as an indirect measure of their ability to adsorb cations and, more broadly, to
404 electrochemically react with the pore solution since the electrical double (triple) layer is directly
405 linked to counter cations adsorption. The objective of this preliminary selection is to handle a
406 panel of samples representative of a wide range of CEC values and therefore representative of

a wide range of reactive materials. Table 1 shows the CEC values, the clay mineral compositions and the porosity values of these five samples. This illustrates that the higher the content of reactive clay minerals (i.e., montmorillonite) is, the higher the measured CEC value.

In the second stage, five electrical conductivity measurements acquired at five fluid salinities and measured on each of the five preselected samples are considered (see the data in Figures 4a and 4b). These five fluid salinity concentrations correspond to the lowest values of equilibrium solution conductivity from Waxman and Smits's database, i.e., in the range of 2.085 $dS.m^{-1}$ up to 28.22 $dS.m^{-1}$. In this low-salinity range, the bulk of the conductivity of a given rock increases sharply and nonlinearly with the solution conductivity, thus violating Archie's relationship (equation 18) (see the data in Figures 4b). This nonlinear increase in conductivity with the increase in the concentration of electrolytes in the low-salinity range is attributed to the so-called surface conduction or surface effects, as explained previously. In contrast, at high electrolyte concentrations, i.e., in the high-salinity domain corresponding to solution conductivity values greater than 28.22 $dS.m^{-1}$, the rock conductivity increases proportionally with the solution conductivity, i.e., following 1:1 a ratio, as predicted by Archie's relationship (Figure 4a). In this high-salinity domain, the electrical conduction is purely electrolytic, i.e., controlled by the conductivity of the bulk solution. As mentioned previously, the rock conductivity values in the high-salinity domain are not considered in this application.

This selection of electrical data is used to invert the parameters of the fractional DS model, the fractional order α, and the cementation exponent m in the following four cases:

- **Case 1**. Both parameters, the fractional order α and the cementation exponent m, are assumed to be independent of the solution salinity. In other words, they are supposed to be constant for a given rock sample and do not depend on the solution electrical conductivity σ_w. This simplest case is considered as a reference case with regard to the other cases that follow.

- **Case 2.** The cementation exponent m is assumed to be independent of the solution salinity, but the fractional order α nonlinearly evolves with the solution conductivity, following this simple relationship:

$$\alpha = 1 + \frac{\sigma_w^0}{\sigma_w} \tag{43}$$

where the unknown parameter σ_w^0 must be inverted. This case is suggested by experimental observations that show that the formation factor and thus the effective conductivity decrease nonlinearly with the solution conductivity[55, 66] (Figure 2). It can be seen from (43) that for the high-salinity limit, if $\sigma_w \to \infty$, then $\alpha \to 1$, and Archie's relationship is retrieved as expected.

- **Case 3.** The fractional order α is assumed to be independent of the solution salinity, but the cementation exponent m nonlinearly evolves with the solution conductivity, following this simple relationship:

$$m = a + b\, ln\sigma_w \tag{44}$$

where a and b are parameters to be inverted. The particular mathematical form of equation (44) is suggested by the increase in rock conductivity as the solution conductivity increases, as indicated in Figure 4b. This nonlinearity (44) is introduced by the fact that the changes in solution conductivity imply some swelling or shrinkage of the reactive clay aggregates, which in turn should significantly modify the electrical tortuosity and rock microstructure. The impact of this swelling or shrinkage of clay aggregates on transport properties is rarely considered in the literature.

- **Case 4.** Both parameters, the fractional order α and the cementation exponent m, are assumed to be dependent on the solution salinity, following the relationships in (43) and (44).

453 The unknown parameters involved in these four cases are inverted by means of an
454 optimization scheme based on Monte Carlo sampling[77-78], and they are applied to the five
455 electrical conductivity measurements of each of the five preselected samples. This scheme,
456 considered a Markov chain Monte Carlo (MCMC) approach, is a probabilistic technique whose
457 basic principle consists of an oriented random walk exploration of the parameter space to avoid
458 large time-consuming computations. This type of technique is also particularly able to account
459 explicitly for the experimental uncertainties that are assumed to follow a Gaussian distribution
460 (see details in Tarantola[78]).

461 It should be noted that cases 1 and 2 imply that there are two parameters to be inverted,
462 whereas cases 3 and 4 use three parameters, (α, a, b) and (a, b, σ_w^0), respectively. For the
463 objective of carrying out the simplest modeling approach and inverting the same number of
464 unknown parameters for all four cases, the smallest number of parameters (two parameters) is
465 considered in the following analysis. Thus, to invert only two parameters for each of the four
466 cases, an additional assumption is introduced at this stage. It is assumed that the cementation
467 exponent value for the selected sample with the highest solution salinity, i.e., 28.22 dS.m^{-1}, is
468 equal to m_{HS}, which is the cementation exponent value calculated at the highest solution
469 conductivity (i.e., at the highest salinity) found in the Waxman-Smits database, i.e., 233.5
470 dS.m^{-1} (see the m_{HS} values in Table 1). In other words, the cementation exponent is assumed to
471 be constant between 28.22 dS.m^{-1} and 233.5 dS.m^{-1}, i.e., a salinity range for which surface
472 conduction does not impact the electrical tortuosity and rock microstructure. From this
473 assumption, equation (44) can be rewritten as follows:

$$m = m_{HS} + b\ ln\left(\frac{\sigma_w}{28.22}\right) \tag{45}$$

474 where the solution electrical conductivity σ_w is now expressed in dS.m^{-1} and the parameter b is
475 the sole parameter to be inverted.

476 The results of the inversion of each pair of parameters for each of the four cases and for
477 the five selected samples are given in Table 2. To compare the quality of the inversions
478 performed for each case, the root-mean-square error (RMSE) is calculated as follows:

$$RMSE = \sqrt{\frac{1}{n}\sum_{i=1}^{n}\left(\frac{obs_i - sim_i}{obs_i}\right)^2} \quad (46)$$

479 where n is the number of measurements (here, five for each sample) and obs_i and sim_i are the
480 measured and simulated values, respectively, obtained for each measurement i. Note that the
481 MCMC optimization scheme is run at least 50 times for each case, and the inverted values
482 yielding the smallest RMSE (minimum RMSE) are retained as results in Table 2.

483 In a general way, the results in Table 2 reveal the following features. First, case 1 shows
484 the highest minimum RMSE values, greater than 46% for all five samples. Moreover, case 1
485 provides inverted values of both parameters, α and m, over wide ranges, illustrating that several
486 values of these parameters that are very different yield similar minimum RMSE values. The
487 poor agreement between the measured and simulated values and the high uncertainties in the
488 inverted parameters are not surprising. Indeed, case 1 predicts a linear relationship between the
489 solution conductivity σ_w and the effective rock conductivity σ^* (see equation 37, where
490 parameters, α and m, are constant), which is not observed experimentally in this salinity range
491 (Figure 4b). These results highlight, as expected, that the relationships between the parameters
492 α and m and between the solution conductivity and salinity are required to fit the Waxman
493 Smits data.

494 Thus, in comparison with case 1, case 2 noticeably improves the agreement between the
495 measured and simulated values. Table 2 indicates for case 2, the minimum RMSE values are in
496 the range of 14.9-41.6 (%) for all five samples. However, these RMSE values are still high, i.e.,
497 greater than 5%; the improvement of fit is significant in case 3.

Indeed, case 3 shows minimum RMSE values that are lower than 3.15% for all the samples. This satisfactory agreement is displayed in Figures 4a and 4b. The slight disagreement observed for the highest solution conductivity (at 28.22 $dS.m^{-1}$) in Figure 4b is likely because at this salinity, the amplitudes of surface conduction and the related physico-chemical effects are not high.

In contrast with case 3, case 4, which introduces two nonlinearities through equations (43) and (44), does not significantly improve the agreement between the measured and simulated values. The minimum RMSE values provided by case 4 are between 3.16% and 6.49%, and they are greater than those of case 3, which are all lower than 3.16% (Table 2).

If we focus now on the results of case 3, which provides the lowest minimum RMSE values, two comments can be made. First, our inversion results show that the cementation exponent is extremely sensitive to solution conductivity changes (Figure 5). The inverted values of the parameter *m* for all samples significantly increase with solution conductivity. This sensitivity appears to increase with the sample reactivity. Indeed, it reaches its maximum value for sample WS26, which exhibits the highest content of reactive clay minerals (montmorillonite) and thus the highest CEC value, i.e., 1.47 $mequiv.cm^{-3}$ or 0.164 $mequiv.g^{-1}$ (Table 1). The cementation exponent of sample WS26 increases from 0.34 to 2.30. This is an increase of 576% with respect to the initial cementation exponent at the lowest solution conductivity, i.e., 2.085 $dS.m^{-1}$. In contrast, this sensitivity to the solution conductivity is minimal for sample WS17, which has the lowest CEC value, i.e., 0.33 $mequiv.cm^{-3}$ or 0.02 $mequiv.g^{-1}$ (Table 1). The cementation exponent of sample WS17 increases from 0.90 to 1.85. This is an increase of 106% with respect to the initial cementation exponent at the lowest solution conductivity. This increase is five times less than that observed for the WS26 sample. This dependence of the sensitivity of *m* on clay-rock reactivity can be also illustrated in Figure 6 which displays a clear positive correlation between the parameter *b* in equation (45) and the

cation exchange capacity. Consequently, it can be suggested here that the cementation exponent should account for the microstructural evolution associated with the swelling/shrinkage of clay minerals or aggregates directly due to salinity changes in clayey rocks. The microstructural evolution may correspond to changes in pore connectivity and tortuosity and, more generally, to the evolution of the geometric pore space of the clayey rock under study.

Second, the fractional order α is also dependent on the rock reactivity. Figures 6a and 6b indicate that the increase in the parameter α is an almost linear function of the cation exchange capacity. The best agreement between empirical and simulated values is obtained with an exponential function exhibiting a regression coefficient of determination R^2 equal to 0.98 (Figure 7a). It should be noted that an extrapolation of this exponential fit at CEC=0 leads to an α value of 1.02, which close to 1 as expected for a nonreactive rock. Consequently, the results in Figures 7a and 7b suggest that the fractional order α could be an interesting indicator of the amplitude of surface conduction in clayey rocks. To confirm this observation and the previous observations, the fractional DS will be applied to diffusion coefficient data of saturated clay montmorillonite.

However, in order to test the predictive nature of the model, two test cases are performed using two additional samples, named WS21 and WS22 in the Waxman-Smits database. The values of petrophysical properties of these two additional samples are given in Table 3. Parameters α and m (through b of equation (45)) are calibrated by using the non-linear regressions given in Figures 7a. and 6, respectively (see results in Table 3). Figure 8 which displays the results of these two test cases shows that the model satisfactorily predicts the measured data. The RMSE between simulated values and measured values of samples WS21 and WS22 are 9.6 % and 10.6 %, respectively.

3.3 Diffusion coefficient of compacted montmorillonite

547 The fractional DS is applied to diffusion coefficient data of compacted water-saturated
548 bentonite acquired from classical through-diffusion tests performed by Glaus et al.[59]. The clay
549 portion of bentonite is composed essentially of montmorillonite, a smectite-type clay mineral.
550 This set of data is preferred for at least four reasons. First, these data were obtained on
551 montmorillonite, i.e., a swelling clay mineral that is extremely reactive to changes in pore liquid
552 chemistry. Second, the effective diffusion coefficient was measured with Na^+ counter cations,
553 which are known to physico-chemically interact with montmorillonite more strongly than other
554 ions[59-60, 79]. In the work of Glaus et al.[59], their montmorillonite mixture was chemically treated
555 with a NaCl solution to remove all soluble salts and to convert the clay into a Na-form, i.e., a
556 Na-montmorillonite. Third, these data were acquired for a very large range of cation
557 concentrations for the solution in equilibrium with the clayey geomaterial, i.e., over three
558 decades from 10^{-2} M to 1 M. This equilibrium concentration is hereafter called the "external
559 salt concentration". Fourth, this powder was highly compacted to obtain a dry bulk density of
560 1950 $kg.m^{-3}$, i.e., a porosity of 28%. This state of compaction brings us closer to natural rock,
561 the case encountered in the previous section (3.2).
562 Now, following equation (19), a "diffusion" formation factor is defined as follows:

$$F = \frac{D_w}{D^*} \tag{47}$$

563 where D^* is the effective diffusion coefficient of compacted montmorillonite and D_w is the self-
564 diffusion coefficient of bulk liquid water. The coefficient D_w, always greater than D^*, is set to
565 $1.33\ 10^{-9}$ $m^2.s^{-1}$ for the cation Na^+ [80]. In contrast with the previous electrical conductivity σ_w of
566 the bulk solution, which increases with salinity, the coefficient D_w is independent of the external
567 salt concentration[59, 80] and mainly depends on the chemical species under study, which is the
568 cation Na^+ here.
569 Moreover, compared with the effective electrical conductivity, the effective diffusion
570 coefficient of cations in compact clayey geomaterials decreases with increasing external salt

concentration (compare the data in Figure 4a and Figure 9). The classical interpretation of this evolution is derived from the existence of a "surface" diffusion (often called "interlayer" diffusion) of counter cations, which are the cations Na^+ here. This diffusion mechanism, which dominates the overall diffusion in compacted Na-montmorillonite, occurs in the "near-surface" water between smectite clay minerals (i.e., montmorillonite) and free pore water, or in other words, in the electrical double (or triple) layer (EDL or ETL), existing at the charged surface of montmorillonite. This near-surface water in the vicinity of these surfaces is dominant in nanopores and contains more counter cations than the bulk solution to compensate for the excess of fixed negative charges on the surface of montmorillonite. Following Glaus et al.[59], this surface diffusion is driven by the local cation concentration gradient existing between this near-surface water and the surrounding bulk water; it is larger at low external salt concentrations and decreases as the external salt concentration increases. In other words, the larger the external salt concentration in the bulk liquid is, the lower the local cation concentration gradients between near surface water and bulk water and finally the lower the amplitude of surface diffusion.

Similarly to the previous section 3.2, diffusion coefficient data from Glaus et al.[59] has been used to invert the parameters of the fractional DS model, the fractional order, α, and the cementation exponent, m, following four cases:

- **Case 1**. Both parameters, the fractional order, α and the cementation exponent, m, are assumed to be independent of the external salt concentration. This simplest case is again considered as a reference case with regard to the following others.
- **Case 2.** The cementation exponent, m is assumed to be independent of the external salt concentration named here C_w but the fractional order, α, nonlinearly evolves with the solution conductivity, following this simple relationship:

$$\alpha = 1 + \frac{C_w^0}{C_w} \tag{48}$$

where the unknown parameter C_w^0 must be inverted. It can be seen in (48) that for the high-concentration limit, if $C_w \to \infty$, then $\alpha \to 1$, and Archie's relationship is retrieved as expected.

- **Case 3.** The fractional order α is assumed to be independent of the external salt concentration C_w, but the cementation exponent m nonlinearly evolves with C_w, following this relationship:

$$m = a' + b'\, lnC_w \tag{49}$$

where *a'* and *b'* are parameters to be inverted. Similar to the case with electrical conductivity, this nonlinearity (49) is introduced by the fact that the changes in external salt concentration imply some swelling or shrinkage of the reactive clay aggregates, which in turn should significantly modify the diffusional tortuosity and rock microstructure. For the electrical conductivity, it is desirable to conduct the simplest modeling approach and to invert the same number of unknown parameters for all cases. Thus, to invert only two parameters for each of the four cases, an additional assumption is again introduced at this stage. It is assumed that the cementation exponent value at the highest external salt concentration of our selected data, i.e., 1 M, is equal to m_{HS}, that is, the cementation exponent value at the highest concentration limit for which Archie's relationship is satisfied (i.e., for α equal to 1). In this case, the m_{HS} value is calculated as 2.79 by using equation (19). From this additional assumption, equation (49) can be rewritten as follows:

$$m = m_{HS} + b'\, ln\left(\frac{C_w}{C_{HS}}\right) \tag{50}$$

where *b'* is a parameter to be inverted and C_{HS} is equal to 1 M.

- **Case 4.** Both parameters, the fractional order α and the cementation exponent m, are assumed to be dependent on the pore solution salinity, following the relationships in (48) and (50).

The pairs of unknown parameters in these four cases have are inverted for the five values of external salt concentrations from Glaus et al.[59] by running the same optimization scheme used in the previous section (3.2).

The results given in Table 4 indicate that case 4 provides the lowest minimum RMSE value, i.e., the best fit between the selected data and the fractional DS model. Although the minimum RMSE value of 8.94% for case 4 is significant, Figure 9 shows a satisfactory agreement between the data and the model. The fractional DS model associated with the nonlinearities in (48) and (50) correctly captures the cation concentration dependence of the effective diffusion coefficient of compacted Na-montmorillonite.

Figure 10 displays the inversion results of equations (48) and (50) associated with case 4. Figure 10 shows two features. First, similar to the electrical cementation exponent, our inversion results show that the diffusion cementation exponent is sensitive to the external salt concentration. The diffusion cementation exponent nonlinearly increases from almost 0 at a concentration of 10^{-2} M up to 2.79 at 1 M. Our interpretation of this increase is similar to that provided in section 3.2 for the electrical conductivity. The diffusion cementation exponent appears to account for the microstructural evolution associated with swelling clay minerals or aggregates due to concentration changes in the montmorillonite mixture. These microstructural evolutions can be changes in pore connectivity and tortuosity, likely associated with the swelling/shrinkage and/or aggregation/disaggregation processes of montmorillonite minerals. Second, the fractional exponent α sharply decreases with increasing salt concentration. The parameter α decreases from 9.6 at 10^{-2} M to 1.9 at 0.1 M, and it finally converges to almost 1

639 at 1 M, which is the highest concentration value. The parameter α reaches its maximum value
640 at the lowest values of external salt concentrations for which the surface diffusion is maximal.

641 At this stage, it is tempting to compare the inverted values of the parameters *m* and α
642 for both transport properties, i.e., the diffusion coefficient and electrical conductivity. However,
643 this exercise is *a priori* difficult for at least three reasons. First, both transport properties do not
644 refer strictly to the same physico-chemical phenomena, e.g., charge carrier movement driven
645 by a gradient of electrical potential for the electrical conductivity and Brownian movement
646 driven by a gradient of chemical potential for the diffusion coefficient. Second, the salt
647 concentration ranges of the two studies are not strictly similar. Glaus et al.[59] used a wide salinity
648 range from 10^{-2} M to 1 M, while Waxman and Smits[58] used a salinity range from approximately
649 2.10^{-2} M to 0.3 M after converting the solution conductivities to NaCl concentrations using the
650 TDS-total dissolved salt method[81]. Third, a clayey rock and a compacted montmorillonite-rich
651 geomaterial do not have exactly the same microstructure and clay mineral contents. Contrary
652 to the compacted montmorillonite mixture studied by Glaus et al.[59], the clayey rocks in the
653 electrical WS database are not pure clayey material and contain a significant amount of nonclay
654 minerals, e.g., quartz and calcite, whose proportions may reach a few dozen %. Moreover, the
655 microstructure of clayey rocks results from a complex geological story called diagenesis, which
656 involves the mechanical compaction of sediments as well as geochemical processes, i.e., the
657 precipitation and dissolution of minerals.

658 However, in Figure 10, if we look at the *m* and α values in a restricted concentration
659 range ([2.10^{-2}-0.3] M), which corresponds to the WS database, two remarks can be made. First,
660 the *m* values for both properties are almost similar, i.e., between 0 and 2 (compare Figure 5 and
661 Figure 8). In a first-order approach, the "electrical" cementation exponent and the "diffusion"
662 cementation exponent respond in the same manner to changes in salt concentrations and thus
663 are sensitive to the same physico-chemical phenomena. Second, the diffusion α values in Figure

10 are significantly higher than those obtained from the electrical conductivity (compare Figure 7a, Figure 7b, and Figure 10 over the restricted range [2.10^{-2}-0.3] M). Following our physical definition of the parameter α, this would mean that the amplitude of the surface transport of cations resulting from the interactions between hydrated cations and clay minerals would be much higher in Na-montmorillonite than in the clayey rocks under study. This proposition is supported by the mineral composition of the Na-montmorillonite mixture used by Glaus et al., which is much richer in montmorillonite-reactive minerals (more than 98%) than the clayey rocks of the WS database.

4. Conclusion

A new DS called the fractional DS is presented in this paper. This semi-analytical homogenization scheme is introduced to quantitatively investigate the effects of surface physico-chemical phenomena occurring at the pore fluid/solid interface on the effective transport properties of reactive geosystems, e.g., clayey materials. This fractional DS, which requires neither a particular "grain" transport property nor an interfacial zone, is based on two key elements: (i) the concept of realizability of the DS itself and (ii) a fractional integral formulation of the DS for a two-component composite. The formulation of the fractional DS introduces two parameters: a cementation exponent m and a fractional order α. The cementation exponent m is constant for any given material and is inextricably related to the microstructure of the material. The fractional order α accounts for the amplitude of the "surface" transport of cations resulting from the physico-chemical interactions between hydrated cations and swelling clay minerals (i.e., smectite minerals, especially montmorillonite).

The fractional DS is applied to data on electrical conductivity (Waxman and Smits[58]) and diffusion coefficients (Glaus et al.[59]) acquired from natural clayey rocks and a compacted Na-montmorillonite mixture, respectively. These applications show the main following results:

- The fractional DS model is able to correctly capture the dependence of the cation concentration on the effective transport properties of the clayey materials under study if at least one of the parameters (m or α) is nonlinearly related to the external salt concentration of the electrolyte in chemical equilibrium with the pore solution of the materials.
- Considering both effective transport properties, the inverted values the of cementation exponent m nonlinearly increase from almost 0 at the lowest external salt concentration (typically 10^{-2} M) up to values close to 2 at the highest salt concentrations. This evolution is interpreted as resulting from changes in pore connectivity and tortuosity and more generally from evolutions of the geometric pore space likely associated with the swelling/shrinkage and/or aggregation/disaggregation processes of smectite minerals (i.e., montmorillonite).
- Our inversion results on electrical conductivity data show that the inverted values of the parameter α are linearly and positively correlated with the cation exchange capacity values of the clayey rocks under study. This suggests that the fractional order α would be a good indirect indicator of (a) the amplitude of surface conduction in clayey rocks and, more generally, of (b) the physico-chemical reactivity of clayey geomaterials.

This fractional DS model is not intended to replace the numerous conventional models used to quantitatively describe the electrical conductivity and diffusion coefficients of clayey geomaterials. However, it aims to propose a very general and semi-analytical homogenization scheme that accounts for the physico-chemical reactions occurring at the pore fluid/solid interface involved in the transport process, i.e., leading to “surface” transport. Thus, the very general characteristics of this approach naturally make it possible to generalize it to other

714 transport properties (e.g., thermal conductivity, hydraulic conductivity) of porous media seen
715 as two-component composites for which semi-analytical formulations can be expected.
716

717 **Acknowledgments**. We thank the research project "ExCiTING" that is funded by the French
718 National Research Agency (grant agreement ANR-17-CE06-0012). The authors also
719 acknowledge financial support from the European Union (ERDF) and "Région Nouvelle
720 Aquitaine".
721

722 **References**

723 1- Böhm, H. J. (2004). A short introduction to continuum micromechanics. In *Mechanics*
724 *of microstructured materials* (pp. 1-40). Springer, Vienna.
725 2- Bruggeman, D. A. G., Berechnung Verschiederner Physikalischer Konstanten von
726 Hetärogenen Substanzen, Ann. Phys., 24, 636– 679, 1935.
727 3- Norris, A. N. (1985). A differential scheme for the effective moduli of
728 composites. *Mechanics of materials*, *4*(1), 1-16.
729 4- Hashin, Z. (1983). Analysis of Composite Materials—. *Journal of Applied*
730 *Mechanics*, *50*, 481.
731 5- Berryman, J.G., 1995. Mixture theories for rock properties, in Rock Physics and Phase
732 Relations: A Handbook of Physical Constants, Th.J. Arhens (Ed.) AGU reference Shelf
733 3.
734 6- Sen, P. N., Scala, C., & Cohen, M. H. (1981). A self-similar model for sedimentary
735 rocks with application to the dielectric constant of fused glass beads. *Geophysics*, *46*(5),
736 781-795.
737 7- Norris, A. N., Callegari, A. J., & Sheng, P. (1985). A generalized differential effective
738 medium theory. *Journal of the Mechanics and Physics of Solids*, *33*(6), 525-543.

8- Avellaneda, M. (1987). Iterated homogenization, differential effective medium theory and applications. *Communications on Pure and Applied Mathematics*, *40*(5), 527-554.

9- Hashin, Z. (1988). The differential scheme and its application to cracked materials. *Journal of the Mechanics and Physics of Solids*, *36*(6), 719-734.

10- Le Ravalec, M., & Guéguen, Y. (1996). High-and low-frequency elastic moduli for a saturated porous/cracked rock - differential self-consistent and poroelastic theories. *Geophysics*, *61*(4), 1080-1094.

11- Phan-Thien, N., & Pham, D. C. (2000). Differential multiphase models for polydispersed spheroidal inclusions: thermal conductivity and effective viscosity. *International journal of engineering science*, *38*(1), 73-88.

12- Bussian, A. E. (1983). Electrical conductance in a porous medium. *Geophysics*, *48*(9), 1258-1268.

13- Shackelford, C. D., & Daniel, D. E. (1991). Diffusion in saturated soil. I: Background. *Journal of Geotechnical Engineering*, *117*(3), 467-484.

14- Van Loon, L. R., Glaus, M. A., & Müller, W. (2007). Anion exclusion effects in compacted bentonites: towards a better understanding of anion diffusion. *Applied Geochemistry*, *22*(11), 2536-2552.

15- Timothy, J. J., & Meschke, G. (2016). A micromechanics model for molecular diffusion in materials with complex pore structure. *International Journal for Numerical and Analytical Methods in Geomechanics*, *40*(5), 686-712.

16- Sheng, P. (1990). Effective-medium theory of sedimentary rocks. *Physical Review B*, *41*(7), 4507.

17- Berryman, J. G., Pride, S. R., & Wang, H. F. (2002). A differential scheme for elastic properties of rocks with dry or saturated cracks. *Geophysical Journal International*, *151*(2), 597-611.

764 18- Markov, M., Levine, V., Mousatov, A., & Kazatchenko, E. (2005). Elastic properties of
765 double-porosity rocks using the differential effective medium model. *Geophysical*
766 *Prospecting*, *53*(5), 733-754.
767 19- David, E. C., & Zimmerman, R. W. (2011). Elastic moduli of solids containing
768 spheroidal pores. *International Journal of Engineering Science*, *49*(7), 544-560.
769 20- Feng, S., & Sen, P. N. (1985). Geometrical model of conductive and dielectric
770 properties of partially saturated rocks. *Journal of Applied Physics*, *58*(8), 3236-3243.
771 21- De Lima, O. A., & Sharma, M. M. (1992). A generalized Maxwell-Wagner theory for
772 membrane polarization in shaly sands. *Geophysics*, *57*(3), 431-440.
773 22- Chelidze, T. L., & Gueguen, Y. (1999). Electrical spectroscopy of porous rocks: A
774 review—I. Theoretical models. *Geophysical Journal International*, *137*(1), 1-15.
775 23- Cosenza, P., Camerlynck, C., & Tabbagh, A. (2003). Differential effective medium
776 schemes for investigating the relationship between high-frequency relative dielectric
777 permittivity and water content of soils. *Water resources research*, *39*(9).
778 24- Cosenza, P., Ghorbani, A., Revil, A., Zamora, M., Schmutz, M., Jougnot, D., & Florsch,
779 N. (2008). A physical model of the low-frequency electrical polarization of clay
780 rocks. *Journal of Geophysical Research: Solid Earth*, *113*(B8).
781 25- Leroy, P., & Revil, A. (2009). A mechanistic model for the spectral induced polarization
782 of clay materials. *Journal of Geophysical Research: Solid Earth*, *114*(B10).
783 26- Okay, G., Leroy, P., Ghorbani, A., Cosenza, P., Camerlynck, C., Cabrera, J., Florsch N.
784 & Revil, A. (2014). Spectral induced polarization of clay-sand mixtures: Experiments
785 and modeling. *Geophysics*, *79*(6), E353-E375.
786 27- Markov, M., Levin, V., Mousatov, A., & Kazatchenko, E. (2012). Generalized DEM
787 model for the effective conductivity of a two-dimensional percolating
788 medium. *International Journal of Engineering Science*, *58*, 78-84.

28- Markov, M., Levin, V., & Markova, I. (2018). Determination of effective electromagnetic parameters of concentrated suspensions of ellipsoidal particles using Generalized Differential Effective Medium approximation. *Physica A: Statistical Mechanics and its Applications*, *492*, 113-122.

29- Timothy, J. J., & Meschke, G. (2017). Cascade continuum micromechanics model for the effective permeability of solids with distributed microcracks: Self-similar mean-field homogenization and image analysis. *Mechanics of Materials*, *104*, 60-72.

30- De Lima, O. A., & Sharma, M. M. (1990). A grain conductivity approach to shaly sandstones. *Geophysics*, *55*(10), 1347-1356.

31- Revil, A., Cathles III, L. M., Losh, S., & Nunn, J. A. (1998). Electrical conductivity in shaly sands with geophysical applications. *Journal of Geophysical Research: Solid Earth*, *103*(B10), 23925-23936.

32- Revil, A., & Glover, P. W. J. (1998). Nature of surface electrical conductivity in natural sands, sandstones, and clays. *Geophysical Research Letters*, *25*(5), 691-694.

33- Endres, A. L., & Knight, R. J. (1993). A model for incorporating surface phenomena into the dielectric response of a heterogeneous medium. *Journal of colloid and interface science*, *157*(2), 418-425.

34- Levin, V., Markov, M., Mousatov, A., Kazatchenko, E., & Pervago, E. (2017). Effective electromagnetic properties of microheterogeneous materials with surface phenomena. *The European Physical Journal B*, *90*(10), 192.

35- Milton, G. W. (1985). The coherent potential approximation is a realizable effective medium scheme. *Communications in Mathematical Physics*, *99*(4), 463-500.

36- Roscoe, R. (1952). The viscosity of suspensions of rigid spheres. *British journal of applied physics*, *3*(8), 267.

37- Krohn C. E. (1988). Fractal measurements of sandstones, shales and carbonates. *Journal of Geophysical Research: Solid Earth*, 93, 3297-3305.

38- Van Damme, H. (1995), Scale invariance and hydric behaviour of soils and clays, C. R. Acad. Sci., Ser. IIa Sci. Terre Planètes, 320, 665– 681.

39- Ougier-Simonin, A., Renard, F., Boehm, C., & Vidal-Gilbert, S. (2016). Microfracturing and microporosity in shales. *Earth-Science Reviews*, *162*, 198-226.

40- Ma, L., Fauchille, A. L., Dowey, P. J., Pilz, F. F., Courtois, L., Taylor, K. G., & Lee, P. D. (2017). Correlative multi-scale imaging of shales: a review and future perspectives. *Geological Society, London, Special Publications*, *454*(1), 175-199.

41- Sun, H., Mašín D., Najser J., Neděla V., & Navrátilová E.. (2019). Fractal characteristics of pore structure of compacted bentonite studied by ESEM and MIP methods. *Acta Geotechnica* (2019): 1-17.

42- Hashin, Z. (1968). Assessment of the self-consistent scheme approximation: conductivity of particulate composites. *Journal of Composite Materials*, *2*(3), 284-300.

43- Adessina, A., Barthélémy, J. F., & Fraj, A. B. (2020). Micromechanical model for the diffusion properties of materials embedding complex structures. *Mechanics of Materials*, 103404, doi.org/10.1016/j.mechmat.2020.103404.

44- McLaughlin, R. (1977). A study of the differential scheme for composite materials. *International Journal of Engineering Science*, *15*(4), 237-244.

45- Mendelson, K. S., & Cohen, M. H. (1982). The effect of grain anisotropy on the electrical properties of sedimentary rocks. *Geophysics*, *47*(2), 257-263.

46- Landau, L. D., & Lifshitz, E. M. (1960). Electrodynamics of. *Continuous Media*, Oxford, Pergamon Press.

47- Giraud, A., Sevostianov, I., Kushch, V. I., Cosenza, P., Prêt, D., Barthélémy, J. F., & Trofimov, A. (2019). Effective electrical conductivity of transversely isotropic rocks with arbitrarily oriented ellipsoidal inclusions. *Mechanics of Materials*, *133*, 174-192.

48- Archie, G. E. (1942). The electrical resistivity log as an aid in determining some reservoir characteristics. *Transactions of the AIME*, *146*(01), 54-62.

49- Sen, P. N. (1984). Grain shape effects on dielectric and electrical properties of rocks. *Geophysics*, *49*(5), 586-587.

50- Clennell, M. B. (1997). Tortuosity: a guide through the maze. *Geological Society, London, Special Publications*, *122*(1), 299-344.

51- Glover, P. W. (2010). A generalized Archie's law for n phases. *Geophysics*, *75*(6), E247-E265

52- Salem, H. S., & Chilingarian, G. V. (1999). The cementation factor of Archie's equation for shaly sandstone reservoirs. *Journal of Petroleum Science and Engineering*, *23*(2), 83-93.

53- Han, T., Clennell, M. B., Josh, M., & Pervukhina, M. (2015). Determination of effective grain geometry for electrical modeling of sedimentary rocks. *Geophysics*, *80*(4), D319-D327.

54- Yonezawa, F., & Cohen, M. H. (1983). Granular effective medium approximation. *Journal of Applied Physics*, *54*(6), 2895-2899.

55- Worthington, P. F. (1993). The uses and abuses of the Archie equations, 1: The formation factor-porosity relationship. *Journal of Applied Geophysics*, *30*(3), 215-228.

56- Tyagi, M., Gimmi, T., & Churakov, S. V. (2013). Multi-scale micro-structure generation strategy for up-scaling transport in clays. *Advances in water resources*, *59*, 181-195.

57- Rotenberg, B., Marry, V., Salanne, M., Jardat, M., & Turq, P. (2014). Multiscale modelling of transport in clays from the molecular to the sample scale. *Comptes Rendus Geoscience*, *346*(11-12), 298-306.

58- Waxman, M. H., & Smits, L. J. M. (1968). Electrical conductivities in oil-bearing shaly sands. *Society of Petroleum Engineers Journal*, *8*(02), 107-122.

59- Glaus, M. A., Baeyens, B., Bradbury, M. H., Jakob, A., Van Loon, L. R., & Yaroshchuk, A. (2007). Diffusion of ^{22}Na and ^{85}Sr in montmorillonite: Evidence of interlayer diffusion being the dominant pathway at high compaction. *Environmental science & technology*, *41*(2), 478-485.

60- Charlet, L., Alt-Epping, P., Wersin, P., & Gilbert, B. (2017). Diffusive transport and reaction in clay rocks: A storage (nuclear waste, CO2, H2), energy (shale gas) and water quality issue. *Advances in Water Resources*, *106*, 39-59.

61- Miller, K. S., & Ross, B. (1993). *An introduction to the fractional calculus and fractional differential equations*. Wiley.

62- Dutka, J. (1981). The incomplete Beta function—a historical profile. *Archive for history of exact sciences*, vol. 24, 11-29.

63- Abramowitz, M., & Stegun, I. A. (1972). Handbook of Mathematical Functions with Formulas, Graphs, and Mathematical Tables. National Bureau of Standards Applied Mathematics Series 55. Tenth Printing.

64- Dashtian, H., Yang, Y., & Sahimi, M. (2015). Nonuniversality of the Archie exponent due to multifractality of resistivity well logs. *Geophysical Research Letters*, *42*(24), 10-655.

65- Rhoades, J.D., Ratts, P.T.C. & Prather, R.J. 1976. Effects of liquid phase electrical conductivity, water content and surface conductivity on bulk soil electrical conductivity. *Soil Science Society of America Journal*, 40**,** 651–655.

66- Han, T., Best, A. I., Sothcott, J., North, L. J., & MacGregor, L. M. (2015). Relationships among low frequency (2 Hz) electrical resistivity, porosity, clay content and permeability in reservoir sandstones. *Journal of Applied Geophysics*, *112*, 279-289.

67- Waxman, M.H. and Thomas, E.C., 1974. Electrical conductivities in oil-bearing shaly sands: I. The relation between hydrocarbon saturation and resistivity index. II. The temperature coefficient of electrical conductivity. *Society of Petroleum Engineers Journal/* Soc. Pet. Eng. J., 14: 213-225.

68- Cosenza, P., & Korošak, D. (2014). Secondary consolidation of clay as an anomalous diffusion process. *International Journal for Numerical and Analytical Methods in Geomechanics*, *38*(12), 1231-1246.

69- Cosenza, P., Fauchille, A. L., Prêt, D., Hedan, S., & Giraud, A. (2019). Statistical representative elementary area of shale inferred by micromechanics. *International Journal of Engineering Science*, *142*, 53-73.

70- Robinet, J. C., P. Sardini, D. Coelho, J. C. Parneix, D. Prêt, S. Sammartino, and S. Altmann (2012), Effects of mineral distribution at mesoscopic scale on solute diffusion in a clay-rich rock: Example of the Callovo-Oxfordian mudstone (Bure, France), *Water Resources Research*, 48, W05554, doi:10.1029/2011WR011352.

71- Fauchille, A.-L., 2015. Déterminismes microstructuraux et minéralogiques de la fissuration hydrique dans les argilites de Tournemire : apports couplés de la pétrographie quantitative et de la corrélation d'images numériques. Ph-D Thesis University of Poitiers, France (in French).

72- Philipp, T., Amann-Hildenbrand, A., Laurich, B., Desbois, G., Littke, R., & Urai, J. L. (2017). The effect of microstructural heterogeneity on pore size distribution and permeability in Opalinus Clay (Mont Terri, Switzerland): insights from an integrated

study of laboratory fluid flow and pore morphology from BIB-SEM images. *Geological Society, London, Special Publications*, *454*(1), 85-106.

73- Mercury, L., Vieillard, P., & Tardy, Y. (2001). Thermodynamics of ice polymorphs and 'ice-like'water in hydrates and hydroxides. *Applied Geochemistry*, *16*(2), 161-181.

74- Sposito, G. (2008). *The chemistry of soils*. Oxford university press.

75- Gonçalvès, J., Rousseau-Gueutin, P., De Marsily, G., Cosenza, Ph., & Violette, S. (2010). What is the significance of pore pressure in a saturated shale layer? *Water Resources Research*, *46*(4).

76- Meunier, A. (2005). *Clays*. Springer Science & Business Media.

77- Mosegaard, K., & Tarantola, A. (2002). Probabilistic approach to inverse problems. *International Geophysics Series*, *81*(A), 237-268.

78- Tarantola, A. (2005). *Inverse problem theory and methods for model parameter estimation* (Vol. 89). siam.

79- Kozaki, T., Fujishima, A., Sato, S., & Ohashi, H. (1998). Self-diffusion of sodium ions in compacted sodium montmorillonite. *Nuclear Technology*, *121*(1), 63-69.

80- Li Y.H.., & Gregory, S. (1974). Diffusion of ions in sea water and in deep-sea sediments. *Geochimica et cosmochimica acta*, *38*(5), 703-714

81- Santamarina, J. C., Klein, K. A., & Fam, M. A. (2001). *Soils and waves*. New York: J. Wiley & Sons.

Table captions

Table 1. Ages, compositions of clay fractions (<2μm), values of porosity, the cementation exponent m_{HS}, cation exchangeable capacities Q_v (in milliequivalents per cm^3 of pore volume of the rock), and CECs (in milliequivalents per g^{-1} of dry solid) of the investigated samples[58]. The cementation exponent m_{HS} is calculated at the highest pore solution conductivity (i.e., at the highest salinity) at which surface conduction can be considered negligible.

Table 2. Calculated minimum RMSE values and inverted values of the parameters of the fractional DS model for all modeling cases with the five samples from the Waxman-Smits database.

Table 3. Ages, compositions of clay fractions (<2μm), values of porosity, the cementation exponent m_{HS}, cation exchangeable capacities Q_v (in milliequivalents per cm^3 of pore volume of the rock), calibrated values of parameters α and b (in equation (45)) of the two samples used in test cases.

Table 4. Calculated minimum RMSE values and inverted values of the parameters of the fractional DS model from measurements of the effective diffusion coefficient by Glaus et al.[59].

Figure captions

Figure 1. Natural logarithm of the formation factor, lnF, as a function of the fractional exponent α. The black and gray lines correspond to cementation exponent values of $m=2.7$ and $m=0.2$, respectively. The dashed and solid lines correspond to porosity values of $\phi=0.5$ and $\phi=0.05$, respectively.

Figure 2. Formation factor, F as a function of the porosity ϕ on a log-log scale. The black solid line is Archie's relationship with $m=2$. The black dashed lines correspond to the fractional DS model with $m=2$ and α values ranging from 1.2 to 5. The gray dashed lines correspond to the empirical model of Worthington[55] with pore solution conductivity values ranging from 1 $S.m^{-1}$ to 20 $S.m^{-1}$.

Figure 3a. Equivalent grain size distribution (modified from Fauchille[71]).

Figure 3b. Equivalent pore size distribution (modified from Ougier-Simonin et al.[39]).

Figure 4a. Measured rock conductivity as a function of solution conductivity. The gray area indicates the transition zone between the low-salinity domain and the high-salinity

961 domain. The fit with the fractional DS model (case 3) and the 1:1 line (dashed line) are
962 also shown.
963 Figure 4b. Measured rock conductivity as a function of solution conductivity in the low-salinity
964 domain. The fit with the fractional DS model (case 3) is also shown.
965 Figure 5. Cementation exponent *m* as a function of solution conductivity (equation (45); for the
966 inverted parameters α and *b* of the DS model for case 3, see Table 2). The dashed lines
967 show the corresponding logarithmic fits.
968 Figure 6. Inverted parameter *b* in equation (45) as a function of the cation exchange capacity
969 Q_v expressed in meq. cm^{-3}. A logarithmic fit is also shown as dashed lines.
970 Figure 7a. Inverted parameter α (model, case 3) as a function of the cation exchange capacity
971 Q_v expressed in meq. cm^{-3}. A linear and an exponential fit are also shown as dashed
972 lines.
973 Figure 7b. Inverted parameter α (model, case 3) as a function of the CEC expressed in
974 $meq.g^{-1}$. A linear and an exponential fit are also shown as dashed lines.
975 Figure 8. Test cases. Measured and predicted rock conductivity as a function of solution
976 conductivity in the low-salinity domain.
977 Figure 9. Measured effective coefficient of diffusion as a function of external salt concentration
978 from Glaus et al.[59]. The fit with the fractional DS model (case 4) is also shown.
979 Figure 10. Inverted fractional order α and inverted cementation exponent *m* as a function of
980 external salt concentration.
981
982
983

Sample	Age	Kaolinite (%)	Illite (%)	Montmorillonite (%)	Porosity (%)	Cementation exponent m_{HS} (-)	Cation Exchangeable Capacity Q_v (mequiv.cm^{-3})	Cation Exchangeable Capacity CEC (mequiv.g^{-1})
WS17	Eocene	100	_	_	14.0	1.85	0.33	0.020
WS19	Albian	20	40	20	25.9	2.0	0.59	0.078
WS23	Lower Tertiary	8	8	84	24.2	2.2	1.04	0.125
WS24	Lower Tertiary	12	8	80	21.6	2.3	0.81	0.084
WS26	Lower Tertiary	_	_	100	22.9	2.3	1.47	0.164

Table 1. Ages, compositions of clay fractions (<2μm), values of porosity, the cementation exponent m_{HS}, cation exchangeable capacities Q_v (in milliequivalents per cm^3 of pore volume of the rock), and CECs (in milliequivalents per g^{-1} of dry solid) of the five investigated samples[58]. The cementation exponent m_{HS} is calculated at the highest pore solution conductivity (i.e., at the highest salinity) at which surface conduction can be considered negligible.

Sample	Case 1			Case 2			Case 3			Case 4		
	Minimum RMS Error (%)	Parameter α (–)	Parameter m (–)	Minimum RMS Error (%)	Parameter σ_w^0 (S.m^{-1})	Parameter m (–)	Minimum RMS Error (%)	Parameter α (–)	Parameter b (–)	Minimum RMS Error (%)	Parameter σ_w^0 (S.m^{-1})	Parameter b (–)
WS17	46.23	1.00-4.72	1.40-2.65	14.86	8.45-8.79	1.79-1.80	2.23	1.27	0.36	3.54	6.60-6.62	0.13-0.14
WS19	38.90	1.06-8.69	1.56-2.66	20.44	11.34-11.69	1.87-1.88	2.22	1.31-1.32	0.41	3.16	7.04-7.11	0.26
WS23	50.67	1.01-4.47	1.45-2.52	36.00	12.84-13.27	1.74-1.75	2.80	1.86-1.87	0.65	6.05	18.07-18.19	0.52
WS24	52.42	1.02-5.34	1.58-2.64	34.19	12.51-12.63	1.94	3.15	1.65	0.62	6.49	13.38-13.53	0.45
WS26	55.69	1.01-5.41	1.40-2.30	41.63	13.98-14.45	1.72	1.43	2.30	0.75	5.24	28.00-28.19	0.65

992 Table 2. Calculated minimum RMSE values and inverted values of the parameters of the fractional DS model for all modeling cases with the five
993 samples from the Waxman-Smits database.

994
995

Sample	Age	Kaolinite (%)	Illite (%)	Montmorillonite (%)	Porosity (%)	Cementation exponent m_{HS} (-)	Cation Exchangeable Capacity Q_v (mequiv.cm^{-3})	Calibrated parameter α	Calibrated parameter *b* in equation (45)
WS21	Lower Tertiary	12	8	80	23.8	1.8	0.29	1.20	0.29
WS22	Lower Tertiary	12	8	80	22.5	2.3	0.72	1.53	0.54

Table 3. Ages, compositions of clay fractions (<2μm), values of porosity, the cementation exponent m_{HS}, cation exchangeable capacities Q_v (in milliequivalents per cm^3 of pore volume of the rock), calibrated values of parameters α and b (in equation (45)) of the two samples used in test cases.

Case 1			Case 2			Case 3			Case 4		
Minimum RMS Error (%)	Parameter α (–)	Parameter m (–)	Minimum RMS Error (%)	Parameter C_w^0 (M)	Parameter m (–)	Minimum RMS Error (%)	Parameter α (–)	Parameter b' (–)	Minimum RMS Error (%)	Parameter C_w^0 (M)	Parameter b' (–)
62.54	7.07-9.39	4.10-4.21	53.09	0.45-0.46	2.96-2.97	17.06	1.10	0.63	8.94	8.59 10^{-1}	0.63

Table 4. Calculated minimum RMSE values and inverted values of the parameters of the fractional DS model from measurements of the effective diffusion coefficient by Glaus et al.[59].

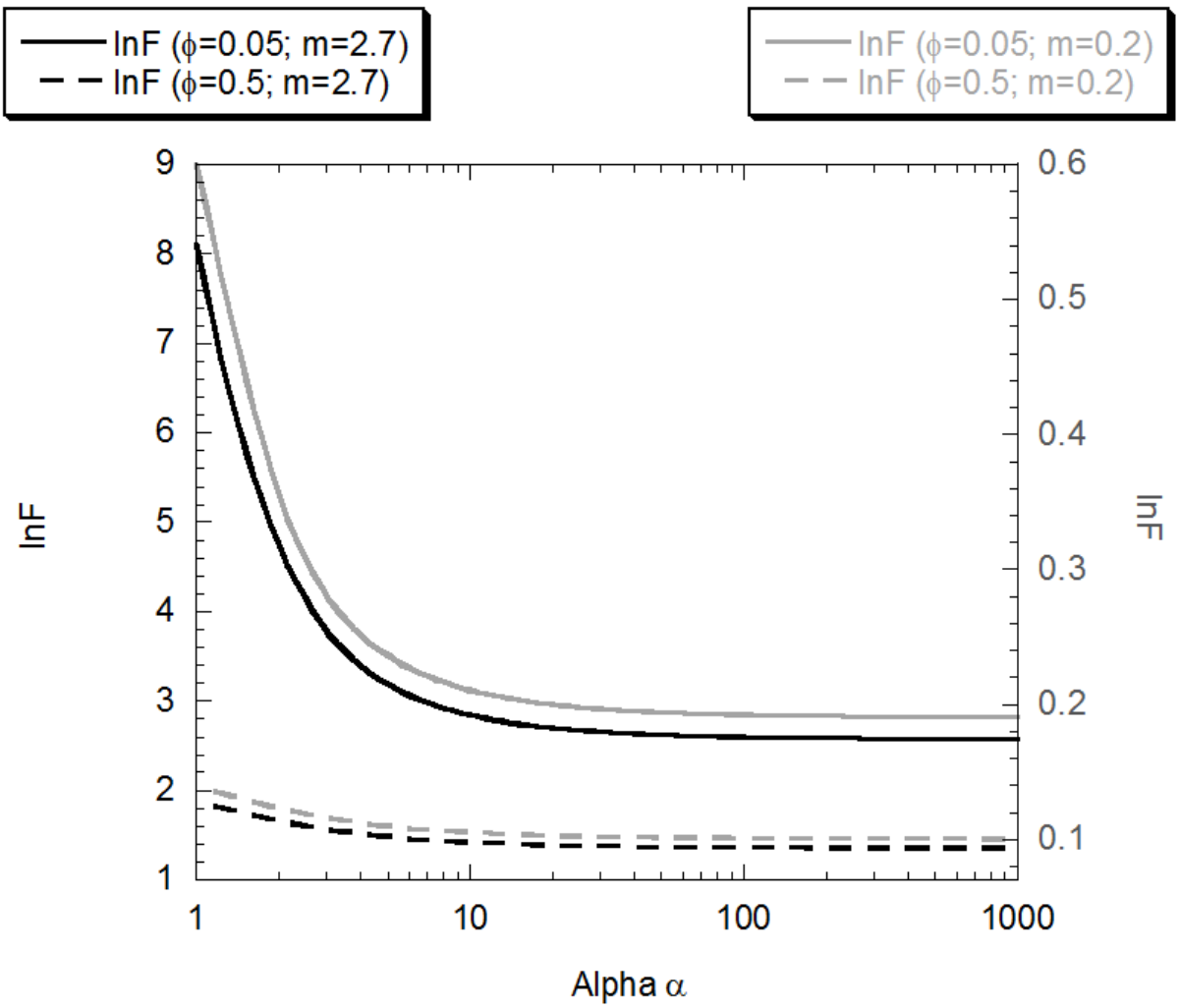

Figure 1 Natural logarithm of the formation factor, *lnF*, as a function of the fractional exponent α. The black and gray lines correspond to cementation exponent values of $m=2.7$ and $m=0.2$, respectively. The dashed and solid lines correspond to porosity values of $\phi=0.5$ and $\phi=0.05$, respectively.

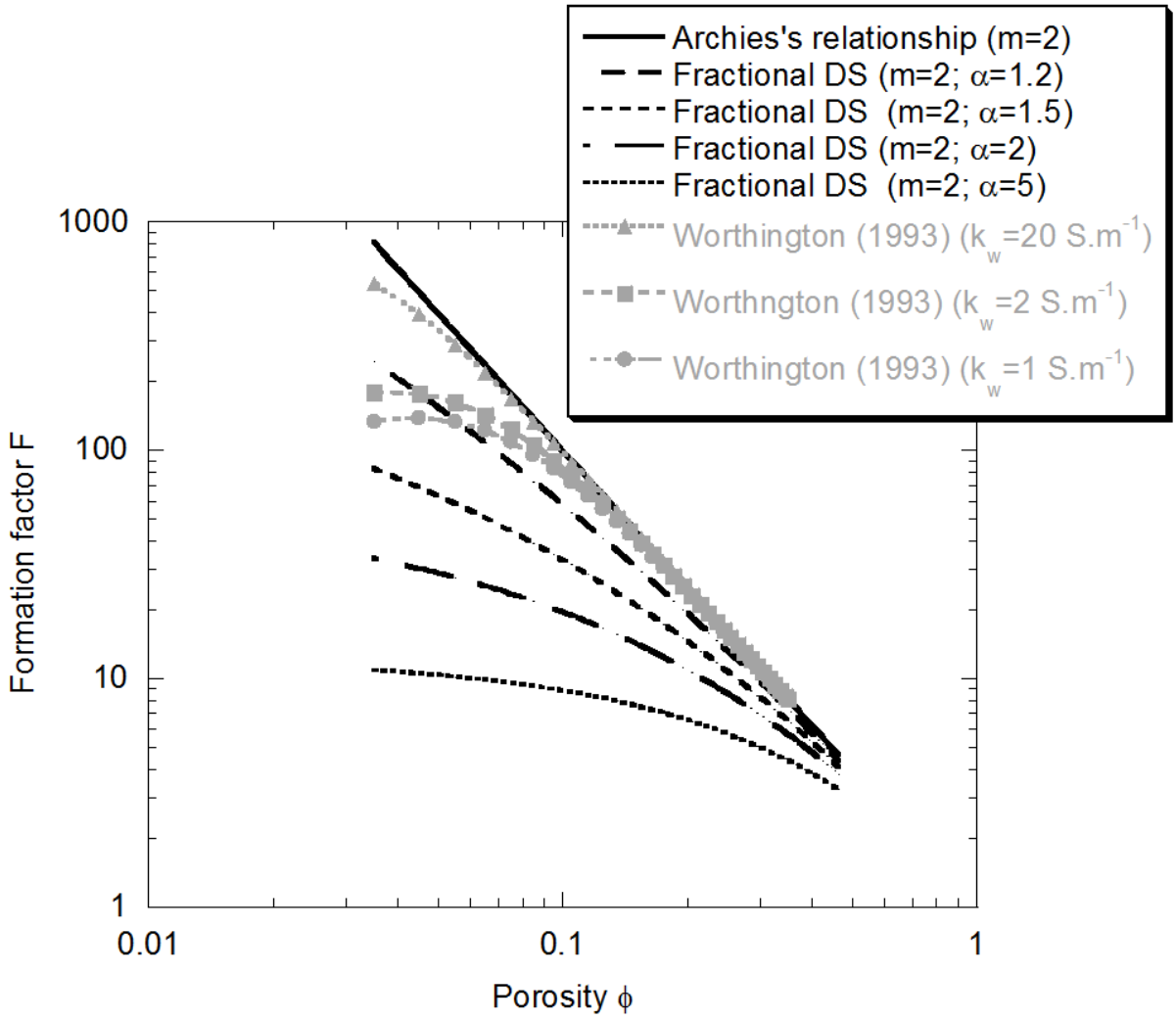

Figure 2. Formation factor, F as a function of the porosity ϕ on a log-log scale. The black solid line is Archie's relationship with $m=2$. The black dashed lines correspond to the fractional DS model with $m=2$ and α values ranging from 1.2 to 5. The gray dashed lines correspond to the empirical model of Worthington[55] with pore solution conductivity values ranging from 1 S.m^{-1} to 20 S.m^{-1}.

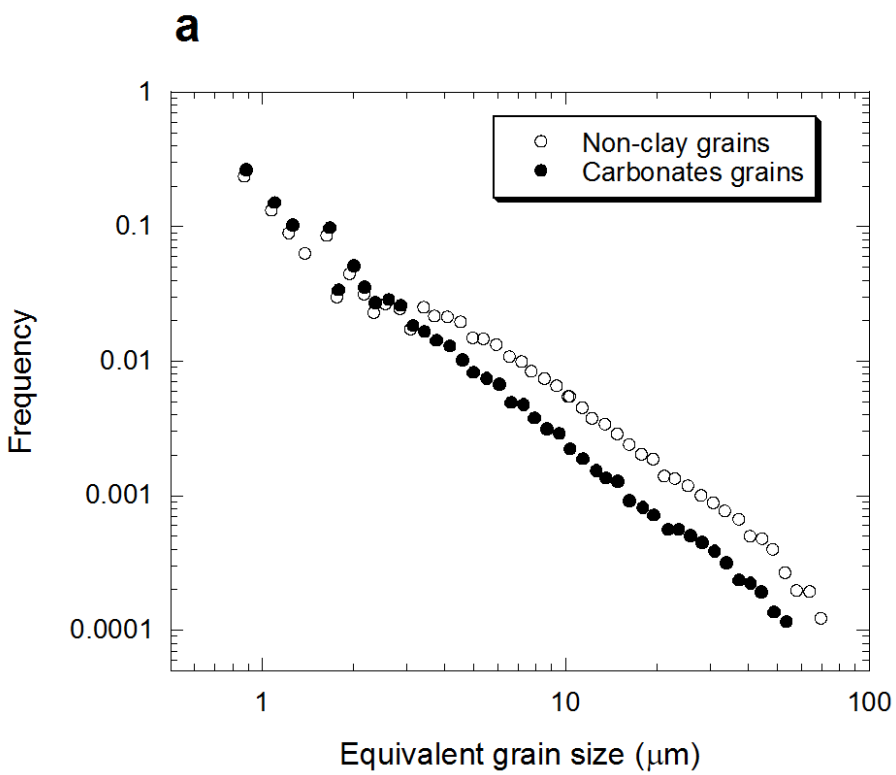

Figure 3a. Equivalent grain size distribution (modified from Fauchille[71]).

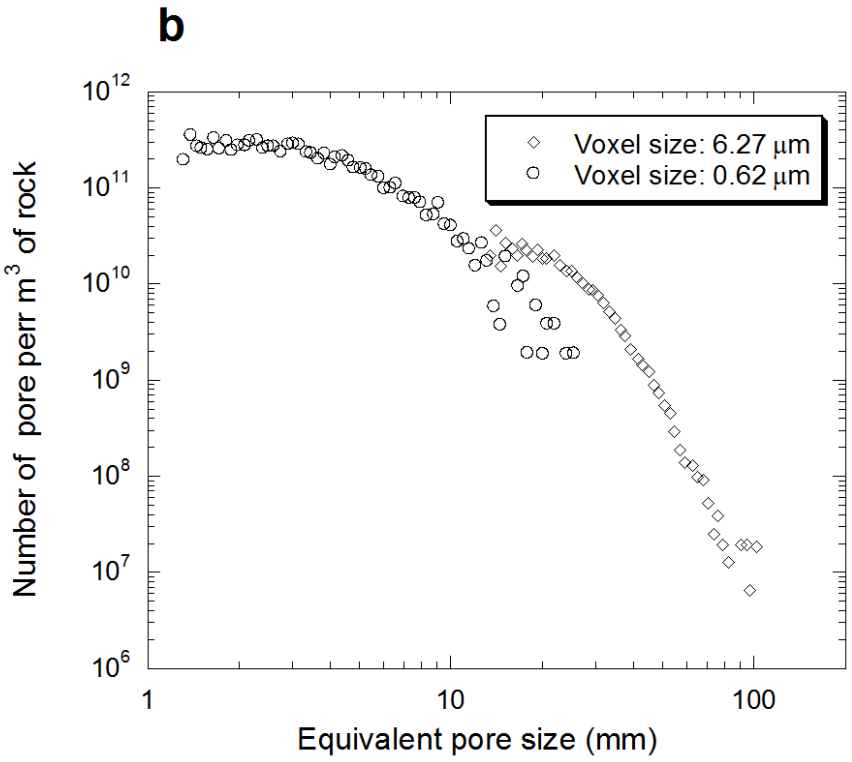

Figure 3b. Equivalent pore size distribution (modified from Ougier-Simonin et al.[39]).

1026

1027

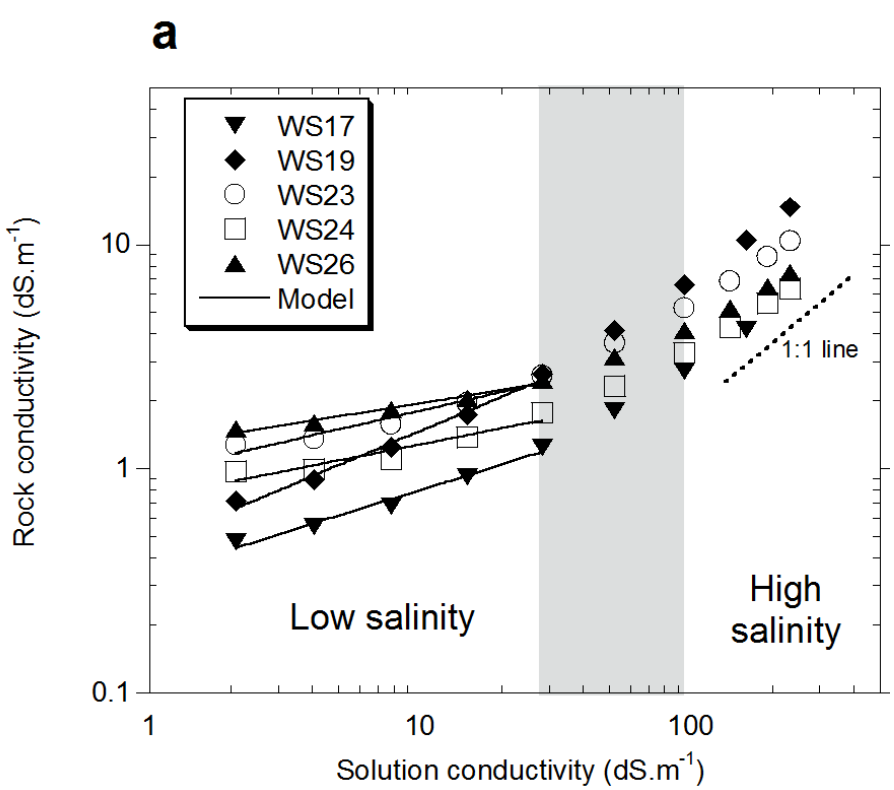

Figure 4a. Measured rock conductivity as a function of solution conductivity. The gray area indicates the transition zone between the low-salinity domain and the high-salinity domain. The fit with the fractional DS model (case 3) and the 1:1 line (dashed line) are also shown.

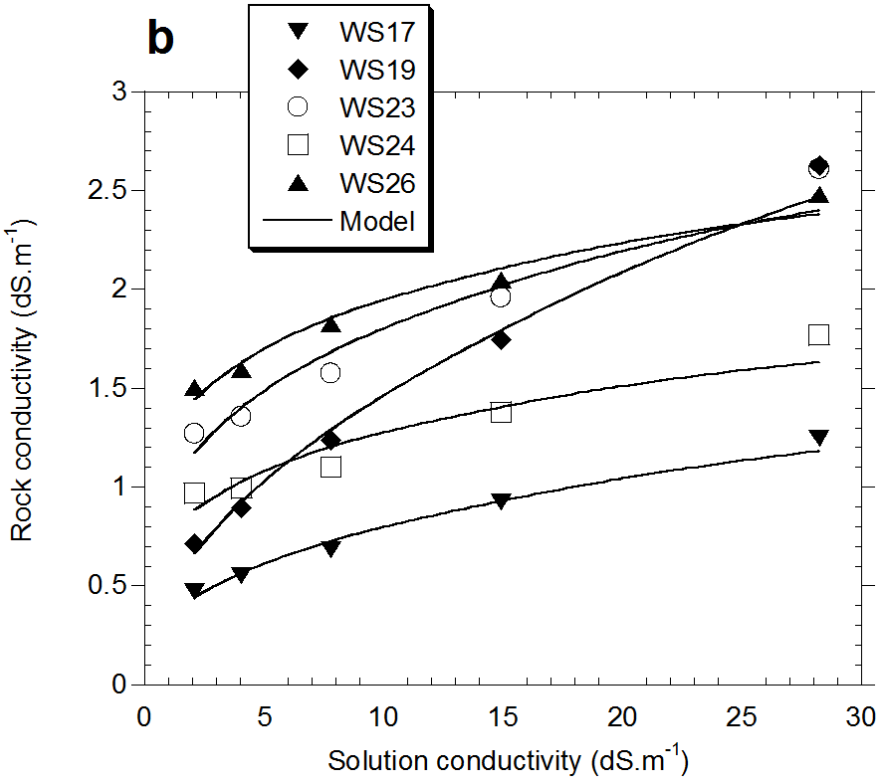

Figure 4b. Measured rock conductivity as a function of solution conductivity in the low-salinity domain. The fit with the fractional DS model (case 3) is also shown.

.

1028

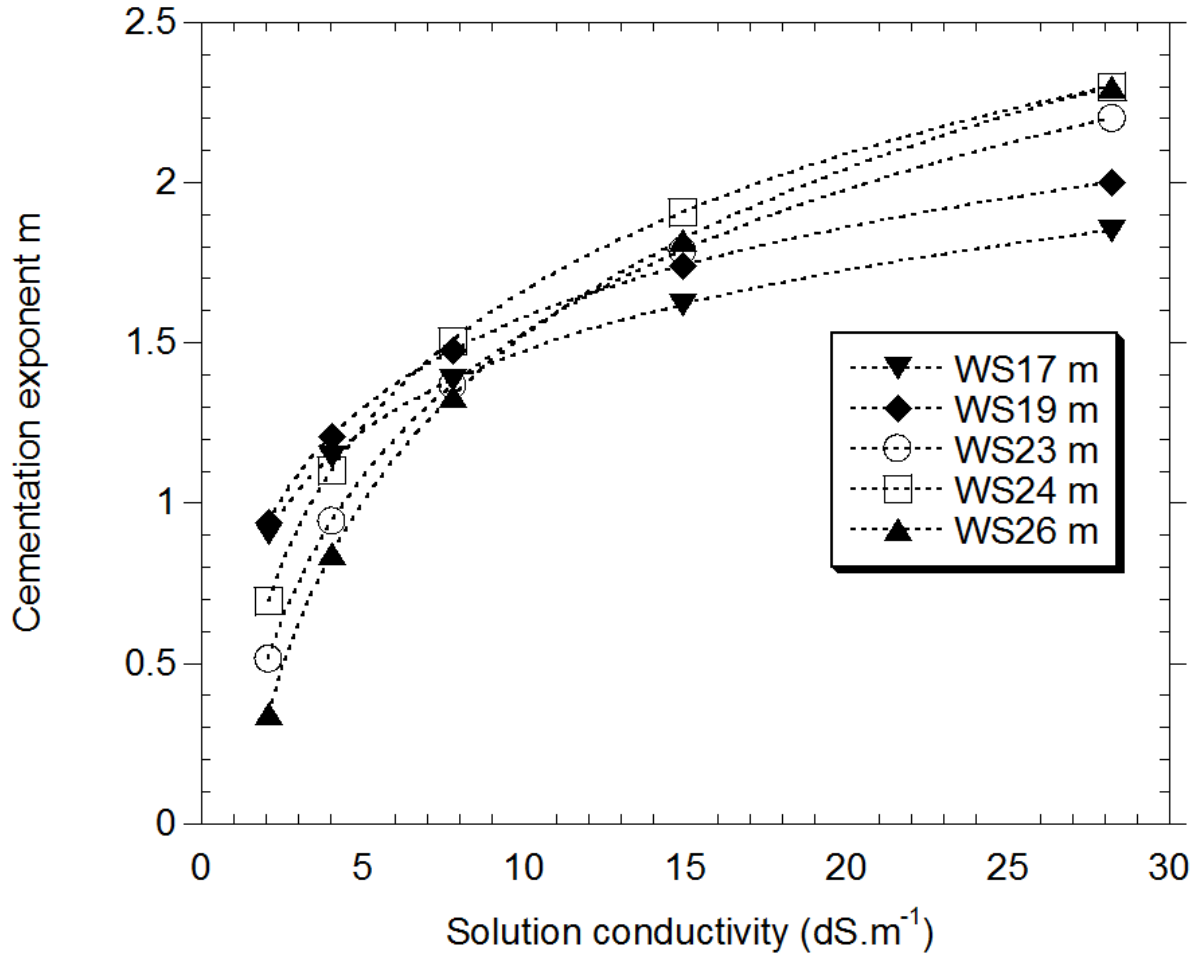

Figure 5. Cementation exponent *m* as a function of solution conductivity (equation (45); for the inverted parameters α and *b* of the DS model for case 3, see Table 2). The dashed lines show the corresponding logarithmic fits.

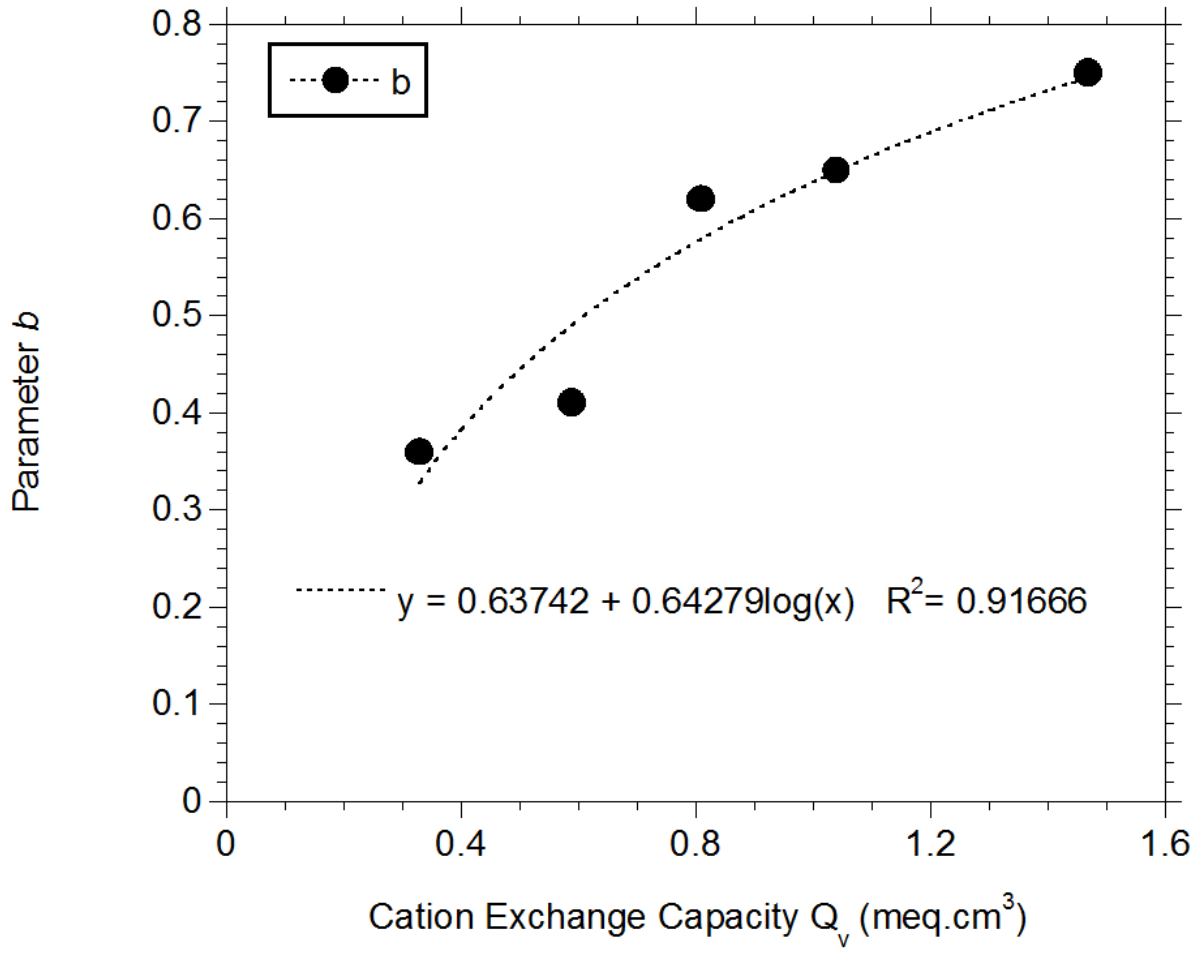

Figure 6. Inverted parameter *b* in equation (45) as a function of the cation exchange capacity Q_v expressed in meq. cm^{-3}. A logarithmic fit is also shown as dashed lines.

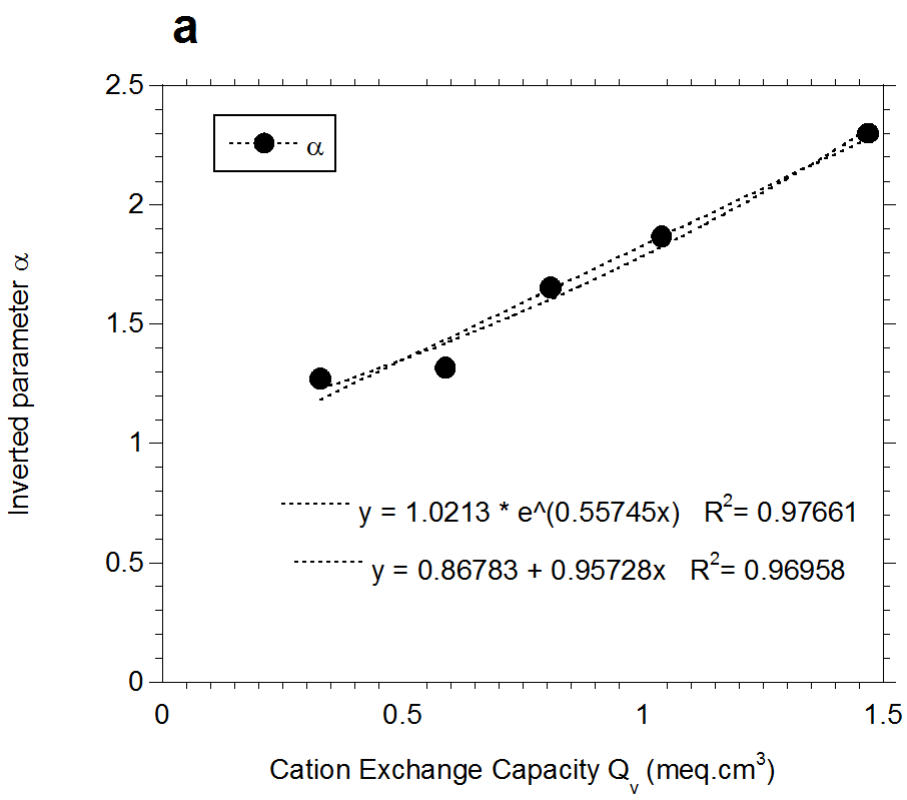

Figure 7a. Inverted parameter α (model, case 3) as a function of the cation exchange capacity Q_v expressed in meq. cm^{-3}. A linear and an exponential fit are also shown as dashed lines.

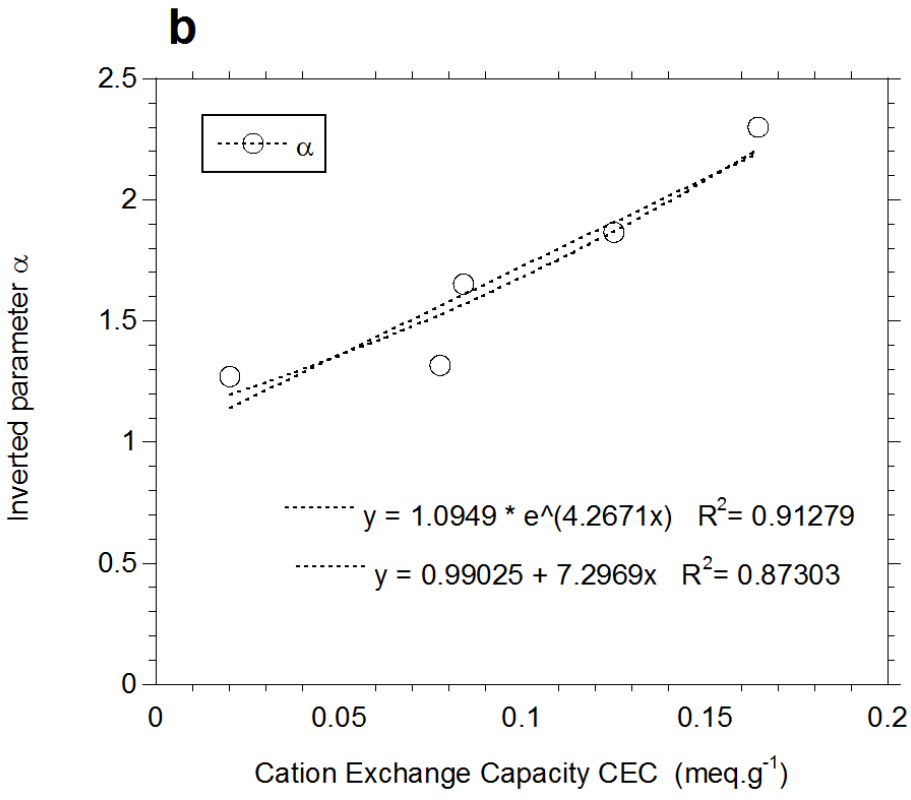

Figure 7b. Inverted parameter α (model, case 3) as a function of the CEC expressed in $meq.g^{-1}$. A linear and an exponential fit are also shown as dashed lines.

1039

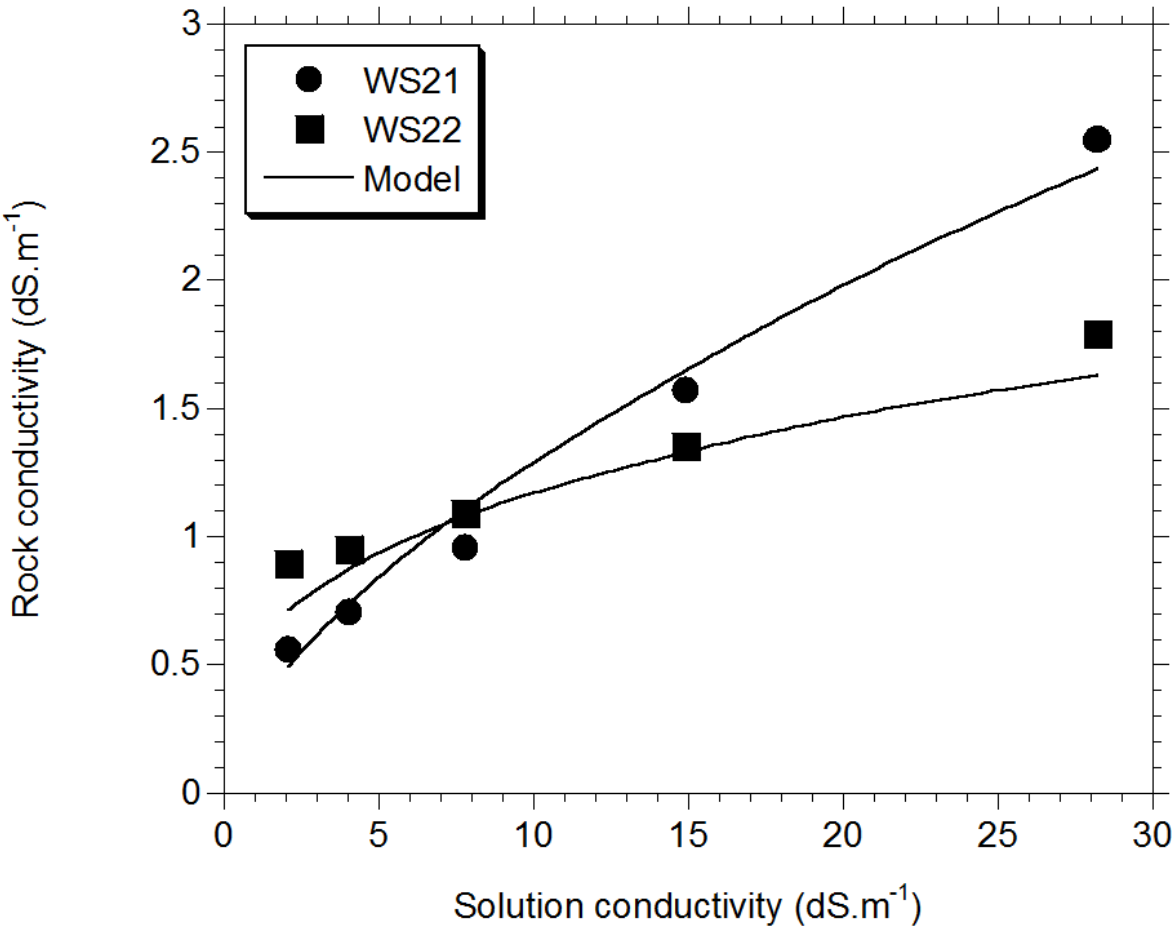

1040

1041 Figure 8. Test cases. Measured and predicted rock conductivity as a function of solution
1042 conductivity in the low-salinity domain.

1043

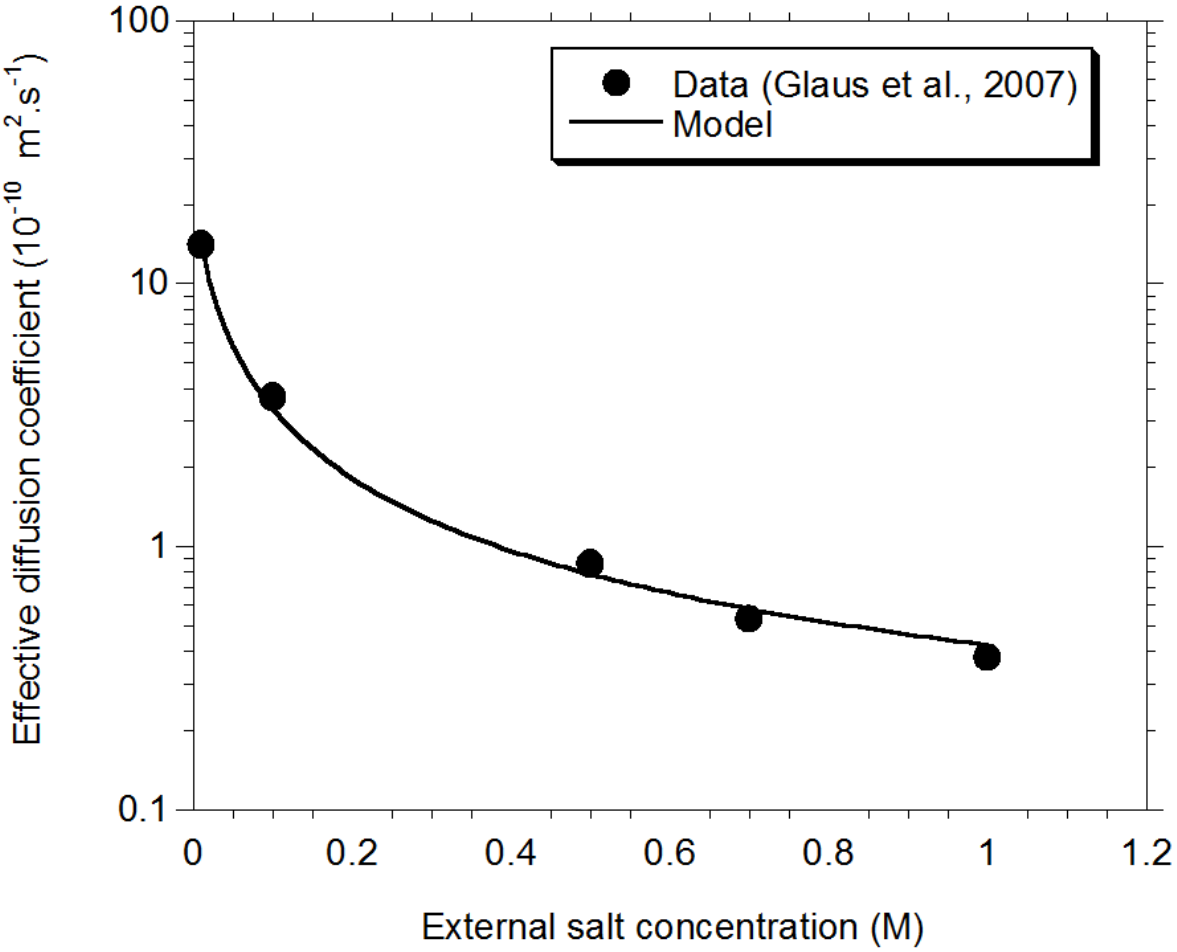

Figure 9. Measured effective coefficient of diffusion as a function of external salt concentration from Glaus et al.[59]. The fit with the fractional DS model (case 4) is also shown.

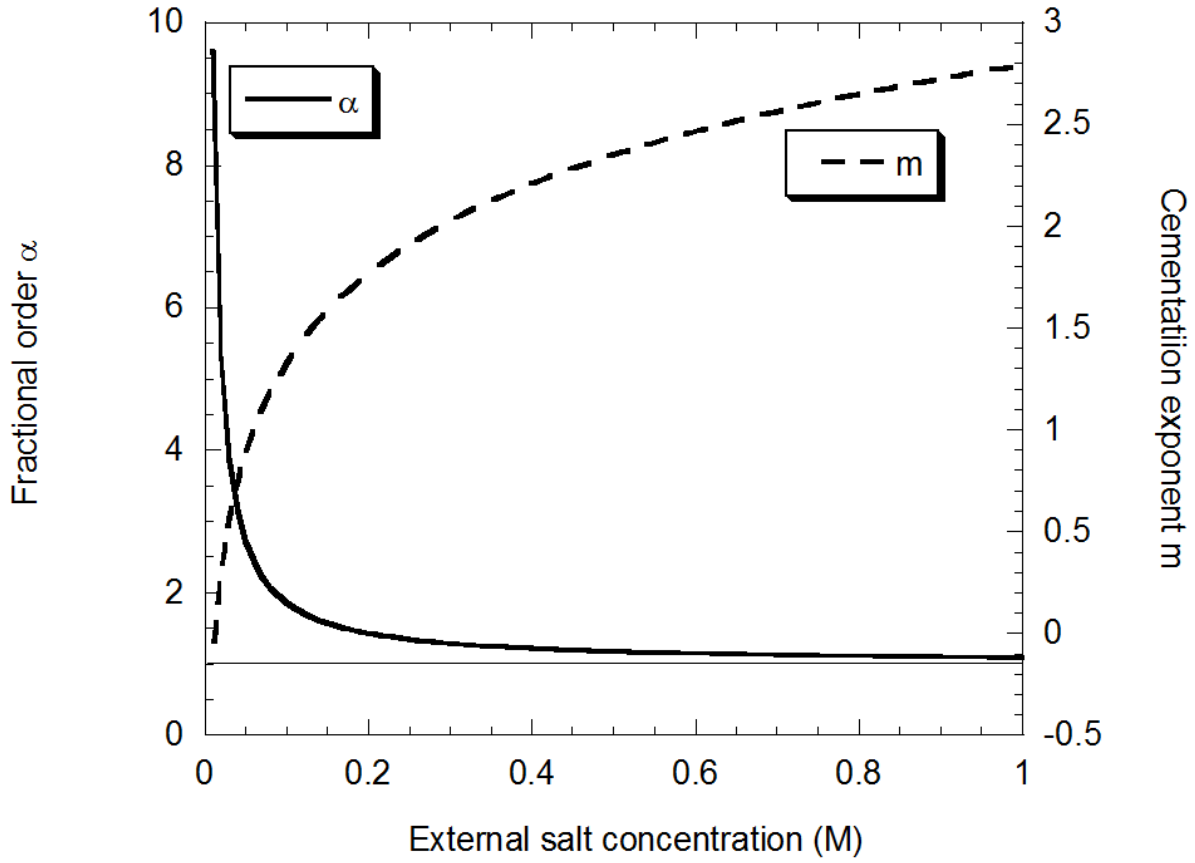

Figure 10. Inverted fractional order α and inverted cementation exponent m as a function of external salt concentration.